



Post-fire management effects on sediment (dis)connectivity in Mediterranean forest ecosystems: Channel and catchment response

Javier González-Romero¹  | Manuel López-Vicente² | Elena Gómez-Sánchez¹ | Esther Peña-Molina¹ | Pablo Galletero¹ | Pedro Plaza-Alvarez¹ | Daniel Moya¹ | Jorge De las Heras¹ | Manuel Esteban Lucas-Borja¹ 

¹Technical School of Agricultural and Mountain Engineering (ETSIAM), University of Castilla-La Mancha (UCLM), Albacete, Spain

²Group Aquaterra, Advanced Scientific Research Center, University of A Coruña, CICA-UDC, La Coruña, Spain

Correspondence

Javier González-Romero, Technical School of Agricultural and Mountain Engineering (ETSIAM), University of Castilla-La Mancha (UCLM), Albacete 02071, Spain.
Email: javier.gromero@uclm.es

Funding information

European Cooperation in Science and Technology, Grant/Award Number: CA18135; European Social Fund, Grant/Award Number: Sbpj/16/180501/000109; Instituto Nacional de Investigación y Tecnología Agraria y Alimentaria, Grant/Award Number: RTA2017-00042-C05-00

Abstract

Forest fires and post-fire practices influence sediment connectivity (SC). In this study, we use the ‘aggregated index of connectivity’ (AIC) to assess SC in five Mediterranean catchments (198–1090 ha) affected by a wildfire in 2012 in south-eastern Spain. Two temporal scenarios were considered, immediately after the fire and before post-fire management, and 2 years after the fire including all practices (hillslope barriers, check-dams, afforestation, salvage logging and skid trails). One LiDAR (light detection and ranging)-derived digital elevation model (DEM, 2 m × 2 m resolution) was generated, per scenario. The five catchment outlets were established as the computation target (AIC_{OUT}), and structural and functional SC were calculated. Index outputs were normalized to make the results of the non-nested catchments comparable (AIC_{N-OUT}). The output analysis includes the SC distribution along the catchments and at local scale (929 sub-catchments, 677 in the burned area), the hillslope and channel measures’ effect on SC, and a sedimentological analysis using observed area-specific sediment yield (SSY) at 10 new (built after post-fire practices) concrete check-dams located in the catchments ($SSY = 1.94 \text{ Mg ha}^{-1} \text{ yr}^{-1}$; $\sigma = 1.22$). The catchments with more circular shapes and steeper slopes were those with higher AIC_{N-OUT}. The structural SC maps – removing the rainfall erosivity influence – allowed evaluating the actual role played by the post-fire practices that reduced SC ($\bar{x} = -1.19\%$; $\sigma = 0.41$); while functional SC was linked to the actual change of SC ($\bar{x} = +5.32\%$; $\sigma = 0.62$). Hillslope treatments resulted in significant changes on AIC_{N-OUT} at sub-catchment scale with certain disconnectivity. A good and positive correlation was found between the SSY and the changes of AIC_{N-OUT}. However, the coarse DEM resolution explained the lack of effect of the rock check-dams – located on the secondary channels – on AIC_{N-OUT}. AIC_{N-OUT} proved to be a useful tool for decision making in post-fire restoration, but an optimal input data is still necessary to refine calculations.

KEYWORDS

check-dams, disconnectivity, forest fire, post-fire management, sediment connectivity

This is an open access article under the terms of the Creative Commons Attribution-NonCommercial-NoDerivs License, which permits use and distribution in any medium, provided the original work is properly cited, the use is non-commercial and no modifications or adaptations are made.

© 2021 The Authors. *Earth Surface Processes and Landforms* published by John Wiley & Sons Ltd.

1 | INTRODUCTION

Forest fires are regular natural components of some biomes in the Earth's systems and many different plants have developed different mechanisms (e.g., resprout capacity or serotiny) to cope with different fire regimes (Pereira et al., 2018). However, changes in fire recurrence, intensity and severity are currently overcoming ecosystem response capacity to forest fires, which may generate irreversible impacts on soil and vegetation (Hedo et al., 2015). As demonstrated by Vieira et al. (2018), forest fires induce changes in physico-chemical soil properties, which in turn directly alter the catchment hydrological response, increasing soil erosion and sediment delivery. Different research has demonstrated that high-severity fires can reduce the soil's infiltration rates, which can lead to increases in runoff and erosion rates across various locations and ecosystems (e.g., Robichaud et al., 2020). The magnitude of these changes depends on vegetation type (Foster et al., 2019), post-fire precipitation (Wagenbrenner & Robichaud, 2014), pre-fire soil conditions (Tessler et al., 2008) and post-fire management strategies (Vieira et al., 2016).

Overall, post-fire management strategies can trigger or reduce positive and negative impacts on soil and vegetation after wildfires (Pereira et al., 2018). These strategies can be classified in three groups: emergency stabilization, rehabilitation and restoration; and can be planned at channel or hillslope scale (Robichaud et al., 2010). Emergency stabilization techniques are immediately built up after forest fires aiming to decrease runoff generation and velocity, and their associated processes, such as sediment delivery, floods and possible damages to downstream infrastructures (Robichaud et al., 2013). Among the emergency practices, those more usually observed are log erosion barriers, contour felled log debris, mulching or grass seeding at the hillslopes and check-dams in the channels (Fernández et al., 2016). The main rehabilitation and restoration practices include afforestation, which has been widely used in the Mediterranean basin with the objective of watershed protection, using conifers for that purpose (Vallejo & Alloza, 2012). In the last years, new restoration objectives have emerged like increasing biodiversity, and the use of shrubs species in hillslope restoration has been introduced.

Disconnectivity in a system, implies that their components or processes are too remote from each other in space or time, and they do not influence each other, or that a certain threshold must be trespassed to allow connectivity (Wohl et al., 2019). Post-fire management strategies may modify that threshold and imply a certain hydrological disconnectivity as they increase the detention and infiltration of overland flow (Gómez-Sánchez et al., 2019). In fact, different authors demonstrated that post-fire management strategies avoid soil degradation by promoting lower runoff coefficients and erosion rates (Cerdá & Robichaud, 2009; Fernández & Vega, 2016; Lucas-Borja et al., 2019; Shakesby, 2011). In any case, the effectiveness of post-fire hillslope treatments will depend on structure design, the season of the year when built and wildfire severity (Badía et al., 2015; Robichaud et al., 2008). Nowadays, there is still a lack of knowledge regarding their efficiency, which hinders the development of proper restoration strategies (Albert-Belda et al., 2019; Rulli et al., 2013). Some measures, as check-dams, are under debate for being requiring the use of heavy machinery, opening of new trails, and have a high economic cost (Quiñonero-Rubio et al., 2016). Moreover, Boix-Fayos et al. (2008) reported that check-dams produce channel geomorphic

alterations, and Martínez-Murillo and López-Vicente (2018) found more concentrated overland flow patterns associated with new trails. Hillslope bioengineering measures such as log erosion barriers, contour felled log debris or afforestation, require manual operations, the use of field materials, high labour costs and time for the vegetation to growth and cover the soil (Albert-Belda et al., 2019; Frankl et al., 2018). Regarding afforestation, it is usually held that new forest cover decreases the amount and intensity of runoff and that forest litter plays an important role in preventing overland flow and reduces soil erosion (Cerdá & Doerr, 2005; Porto et al., 2009). Consequently, to optimize the use of resources, having a deep understanding of how these measures alter the burned catchments network and a good planning and zoning of the works seems crucial. To do so, new tools which support decision-makers must be considered, among those, sediment connectivity indices have proved to be a very useful one (e.g., López-Vicente et al., 2020; Martínez-Murillo & López-Vicente, 2018; Martini et al., 2020).

The term 'sediment connectivity' (SC) refers to the water-mediated transfer of soil and sediment particles along the landscape features, and can be explained as the connection degree between the sediment sources at any part of the catchment, and the sites where (i) temporal/permanent sedimentation (disconnectivity), and (ii) effective sediment transport take place through the channel network (Hooke, 2003). The SC concept has been thoroughly studied in the last years in Europe thanks to the European Research 'Connecteur' COST action ES1306 (Keesstra et al., 2020). These studies have applied the SC concept to assess the (dis)continuity and intensity of sediment and runoff pathways at hillslope, stream and catchment scales. Two types of SC can be described: Structural connectivity, which is defined by the inherent or potential capacity of a system – conferred by its components – to facilitate or impede sediment transport across the overland flow pathways; and functional connectivity that reflects the system's process dynamics and allows studying the actual transfer of water and sediment within the catchment (Heckmann et al., 2018). Owing to the numerous processes – sometimes simultaneously – involved in the sediment dynamic of a system, its drivers and spatiotemporal patterns, the accurate estimation of SC is a complex task (Turnbull et al., 2018). For that purpose and taking advantage of the increasing availability and quality of remote sensing data, several approaches are available to estimate SC in a variety of physiographic and climatic conditions, such as SedNet (sediment budget model) in agricultural river basins (Smith et al., 2014), RSEDD (revised sediment delivery distributed model) to explore travel time of sediments (Chen & Thomas, 2020), graph theory tools for human-controlled catchments (Fressard & Cossart, 2019), and the application of SC indices (Heckmann et al., 2018). The most widely applied index in the last years has been the IC (index of sediment connectivity) (Borselli et al., 2008) and its subsequent modifications (Cavalli et al., 2013), which has been proven in several countries and environments under different land uses and topographic conditions (Calsamiglia et al., 2018; Chartin et al., 2017; Kalantari et al., 2017). Most studies have usually focused on explanatory and predictive connectivity frameworks which reflect structural SC. In the last years, the trend of the new studies is trying to reflect dynamic processes (functional SC) by working with different temporal resolutions, for example at monthly (López-Vicente & Ben-Salem, 2019) or runoff event (Burguet et al., 2017) scales, using the difference between

digital elevation models (DEMs) to assess geomorphic changes (Heckmann & Vericat, 2018) and adding new variables to existing indices, such as the rainfall erosivity of typhoons (Chartin et al., 2017) or topographic roughness in bare soil areas (Ortíz-Rodríguez et al., 2017). Despite the number of already developed SC approaches and the huge potential of these indices and models to evaluate land management scenarios, there is still a lack of applied research which promote the SC assessment in decision-support systems (Heckmann et al., 2018). In terms of SC assessment after forest fires, several studies have been done in affected Mediterranean (e.g., Calsamiglia et al., 2017; López-Vicente et al., 2020; Martínez-Murillo & López-Vicente, 2018) and humid (Fernández et al., 2020) environments, and also in areas under volcanic influence in Mexico (Ortíz-Rodríguez et al., 2019) or Chile (Martini et al., 2020).

It therefore seems essential to understand how SC at basin scale is affected by distinct post-fire management strategies. In this study, we hypothesized that structural and functional connectivity are significantly reduced by post-fire management strategies at channels and hillslopes, and this effect is observable in the short term (few years after their implementation). This hypothesis is tested in five catchments – affected by an intense wildfire – that drain into main rivers in south-eastern Spain. The catchment outlets are chosen as the computation target, which is linked to the sediment transport dynamic that includes the temporary sediment storage in the channels. To achieve these goals, the aggregated index of connectivity (AIC) is run at two temporal scenarios (pre-management and post-management) and output evaluation is mainly done at small sub-catchment scale and using observed rates of area specific sediment yield (SSY) in check-dams distributed along the stream network. The information herein obtained could lead to better forest management practices to effectively increase post-fire ecosystem management.

2 | MATERIAL AND METHODS

2.1 | Wildfire characteristics and study area

This study was conducted in five forest catchments located in La Sierra de Donceles that extends across the provinces of Albacete and Murcia, near Hellín village (southern Spain) (Figure 1). This area was affected by a wildfire in July 2012. Despite the short duration of the arson fire, c. 24 h (from 1 to 2 July), it burned roughly 6500 ha and fire severity was mainly classified as moderate-high (Gómez-Sánchez et al., 2017, 2019). This certain area has remained unburned for at least 80 years according to the data provided by the Regional Government of Castilla-La Mancha Forest service which also corresponds with the digital cartography generated by the IGN (Spanish Geographic Institute). Nevertheless, other great forest fires have taken place in the surroundings during the last decades, more precisely in the years 1994 and 2000 (Moya et al., 2018).

The five selected catchments were the main catchments of the burned area where the majority of the post-fire measures were built. They were named Postes (C. Pos), Conejo (C. Con), Grillo (C. Gri), Piñero (C. Pin) and Rayares (C. Ray), and present a mountainous relief with elevation ranges from 304 m to 808 m above sea level (a.s.l.). The two south-facing catchments (C. Ray and C. Pin) drain into River Segura, and the three north-facing catchments drain into River Mundo. Moreover, River Mundo drains into Camarillas reservoir, which is located downstream from the burned area (Figure 1). The five catchments area varied between 198 ha (C. Gri) and 1090 ha (C. Pos), and the mean slope values range between 28.9% (C. Pos) and 39.5% (C. Gri) (Table 1). Catchments elongation ratios, defined as the ratio of the diameter of the circle with the same area of the basin and the maximum basin length (Kumar, 2011), varied between 0.525 for C. Gri, which is a very elongated basin, and 0.802 for C. Pin, which

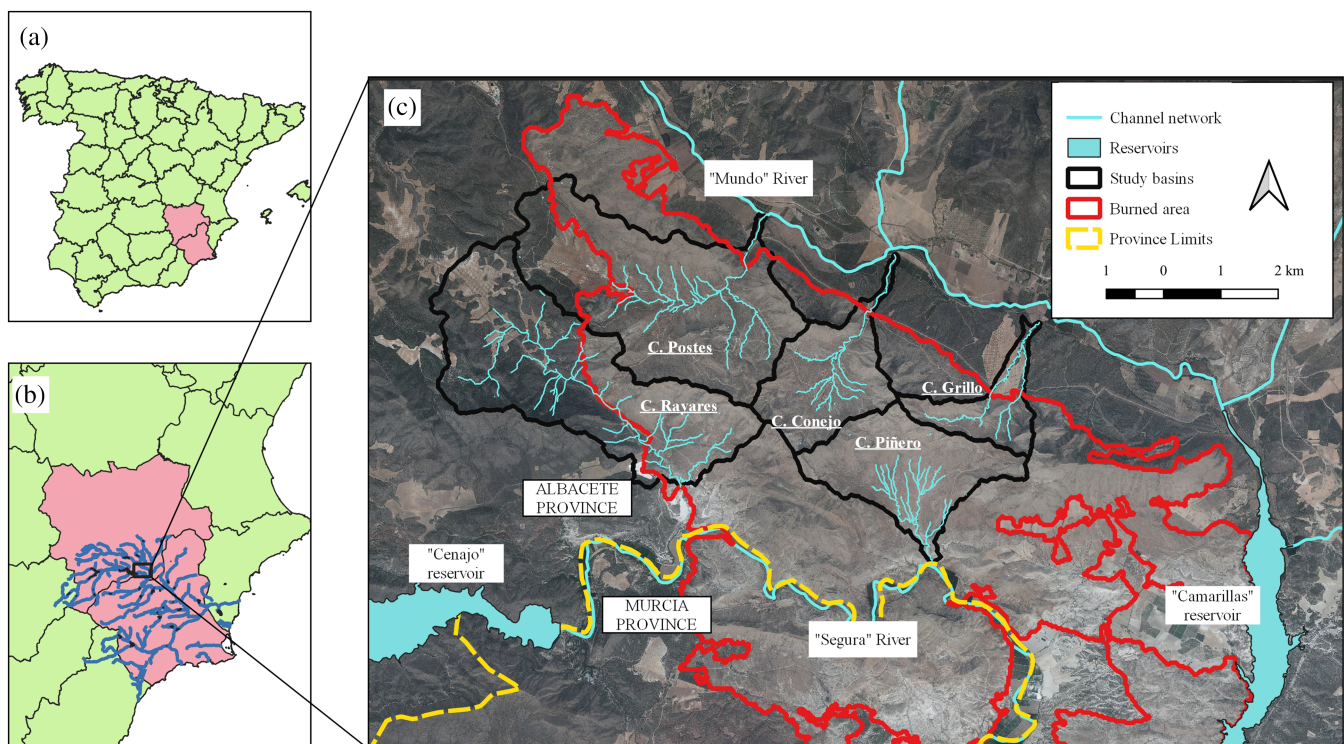


FIGURE 1 (a) Location of Albacete and Murcia provinces (in pink) within Spain. (b) Study area location within the Segura River basin. (c) Location of the burned area and the selected study catchments [Color figure can be viewed at [wileyonlinelibrary.com](https://onlinelibrary.wiley.com)]

TABLE 1 Main physiographic characteristics of the three sub-catchments, including the area occupied by the most important land uses before the wildfire (pre-fire scenario)

Basin (ID)	Area (ha)	Elongation ratio	Slope (%)	Soil permeability class	Predominant aspect class	Forest (ha)	Scrubland (ha)	Pasture (ha)	Arable land (ha)	Tree crops (ha)	Bare soil (ha)	Trails (ha)	Urban areas (ha)
C. Pos	1090	0.637	28.9	Medium-high	Northwest	392.7	276.7	286	31	76	12.4	9.7	5.5
C. Con	388	0.638	38.5	Medium-high	Northwest	131	127	112	8	1	6.5	2.5	ND
C. Gri	198	0.525	39.6	Low-very high	Northwest	63	43	64	0	26	0.95	0.9	ND
C. Pin	495	0.802	37.6	Medium-high	South	49	213	214	0.3	ND	13	4	1.7
C. Ray	1081	0.622	34.1	Medium-high	Southwest	332	309	289	83	27	3.1	6.9	30.5

ND, no data.

resulted as the most circular basin. The maximum lengths of the catchments varied from 5.96 km (B Ray) to 3.02 km (C. Gri).

According to the Soil Taxonomy System, soils belong to the order Aridisol, and to suborder Calcic, showing a loamy – sandy loam soil texture (C.P.B., 1977), its permeability range between medium and very high, appearing sparse low permeability spots in some catchments (IGME – Spanish Geological Survey). Regarding parent materials, Jurassic bedrocks as dolomites, dolomitic limestones or conglomerates appear at the upper areas. At the lower parts, quaternary colluviums appear. The existing streams are mainly narrow (10–20 m), ephemeral (associated with storms and rainy periods), and its streambanks are commonly steep.

The climate is semi-arid Mediterranean, and the area is located on the meso-Mediterranean bioclimatic belt (Rivas-Martínez et al., 2002). The average annual rainfall is c. 320 mm, and the mean annual temperature was 16.2°C for the period 1990–2014 (AEMET – Spanish Agency of Meteorology). The highest rainfall amount is usually recorded during the fall and spring, and summers are very dry.

Before wildfire affection, most of the catchments surface was covered by a *Pinus halepensis* open forest, accompanied by a lush shrub and herbal layer. This conifer forest occupied a wider area at those north-facing catchments (Table 1). In the south-facing catchments, the appearance of the scrub and herbal layers without pines was more common. The shrub layer was mainly composed by species like *Quercus coccifera* and *Pistacia lentiscus* and dwarf shrubs like *Salvia rosmarinus*, *Thymus vulgaris* or *Lavandula latifolia*. Of the herbal layer, if wide, two perennial grasses were the more abundant, *Macrochloa tenacissima* and *Brachypodium retusum*. After wildfire, the vegetation recovery was quite homogeneous for the shrub and herbal layers, in all the catchments due to its pioneer behaviour. Additionally, an incipient pine regeneration was observed in those slopes previously covered by pine forest. Past land management was related to *Macrochloa tenacissima*, which was used as an economic driver from the 17th to the 20th century. Its progressive abandonment and the reforestation action taken by the Public Administrations have shaped a forest landscape composed of *Pinus halepensis*.

Several post-wildfire measures were undertaken during the years following the fire, finishing the works during 2013. Among the different works, two types of measures can be identified: (i) those implemented at hillslopes like log barriers, contour felled log debris or afforestation, and (ii) those built on channels, such as check-dams. These actions took place only in those areas of public domain and their locations are shown in Figure 2 and Table 2.

Hillslope measures mostly took place in those hillslopes where there was enough woody material to build them, as north-facing slopes. In the south-facing hillslopes, some contour felled log debris and afforestation were done. The hillslope measures built after this wildfire were:

I. Hillslope barriers:

- i. Log erosion barriers: The log barriers were built following the contour lines with a maximum length of 15 m and an average distance of 10 m between barriers and a staggered pattern. The logs were fixed with stakes (Figure 2) or with the remaining stumps and had a maximum height of 25 cm or 40 cm if they were located close to a trail or road. Branches were stacked behind the logs acting as an energy dissipater.

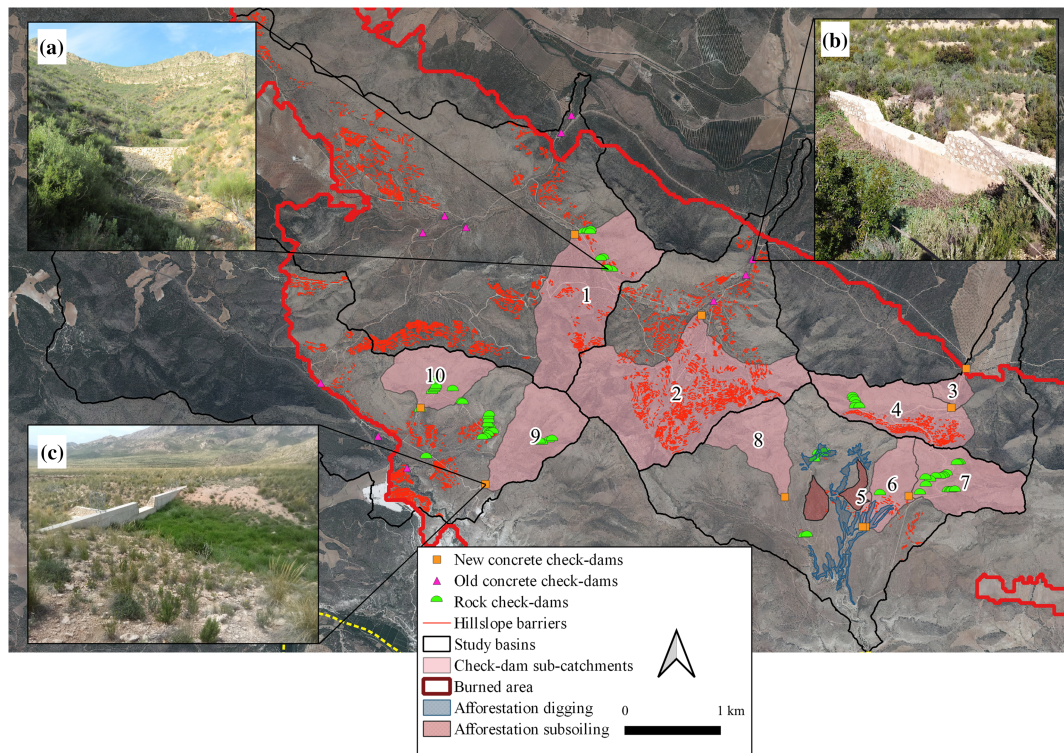


FIGURE 2 Location of the main channel and hillslope measures carried out at the post-fire management. In picture the main channel measures: (a) rock check-dam; (b) old concrete check-dam; (c) new concrete check-dam [Color figure can be viewed at wileyonlinelibrary.com]

TABLE 2 Post-fire management measures density for each catchment

Catchment (ID)	HB density ($m\ ha^{-1}$)	AF area (ha)	RC (number)	NCC (number)	OCC (number)
C. Postes	36.96	—	8	1	5
C. Conejo	86.71	—	—	1	3
C. Grillo	27.05	—	7	2	—
C. Piñero	3.54	35.62	23	4	—
C. Rayares	17.56	—	30	2	3

HB, hillslope barriers; AF, afforestation; RC, small rock check-dams; NCC, new concrete check-dams; OCC, old concrete check-dams.

- ii. Contour felled log debris: Were also disposed following the contour lines and were fixed with stakes.
- II. Afforestation: Two different soil preparation methods were used, mechanical subsoiling, and manual digging. The plantations took place in C. Pin and were carried out using shrub species like *Arbutus unedo*, *Rhamnus lycioides*, *Nerium oleander*, *Salvia rosmarinus*, *Olea europaea* var *sylvestris*, *Phyllirea angustifolia* or *Viburnum tinus*.
- III. Salvage logging: It was carried out with local chainsaw crews and the logs were moved and piled by a small crawler skidder. Several skid trails were opened throughout the treated hillslopes to carry out this works.

Channel measures included two features:

- I. Concrete check-dams (CC): 10 CC were built after the fire and distributed along the five study catchments. CC are mainly thought to protect downslope facilities from floods by trapping sediment and avoiding its delivery out of the catchments. These check-dams have heights between 3 and 6.5 m and widths between 21 and 39 m. All

of them were built at the principal channels of the catchments and close to the main forest roads. Before the forest fire, 12 CC with similar characteristics were already built in the studied catchments. Therefore, the current sediment dynamic in the study area is well regularized and patterns and values do not correspond to the expected natural dynamic without human intervention.

- II. Rock check-dams (RC): A total of 66 RC were built on secondary tributary channels where hillslope vegetation was mostly shrubs and herbal plants, and there was a lack of material to build log barriers at the hillslopes and channels. They have a maximum height of 2 m – depending on the slope of the channel – and in case of building more than one in the same channel the distance between each pair of RCs depends on the RC height and the channel slope, with a minimal distance of 2 m. The used materials were rocks and concrete to make the structure stable (Figure 2).

2.2 | Simulation scenarios and target

The AIC was calculated at two different scenarios, namely:

- I. The 'Pre-Management' scenario (Pre-man; 1 July 2012–30 June 2013). This period was previous to any post-fire management action, representing the situation immediately after the forest fire.
- II. The 'Post-Management' scenario (Post-man; 1 July 2014–30 June 2015) that represents the period when all the post-fire measures were already built, including salvage logging, skid trails, check-dams and hillslope treatments as well as the early vegetation recovery. Afforestation was done in one of the studied catchments (C. Pin) after the wildfire, using two different site preparation techniques (mechanical subsoiling and manual digging). All these measures were considered when preparing index inputs.

The two scenarios were representative of 1-year period starting and finishing in the same date (month and day) of the year, therefore, the represented periods are analogous regarding duration of the hydrological year and vegetation phenology. Among the different computation targets that are usually chosen in this kind of SC studies – the stream system, the basin outlet or any sink (lake, reservoir, check-dam, sinkhole, etc.; more details in López-Vicente et al., 2020) –, to accomplish the aim of this study the basin outlet was chosen (AIC_{OUT}). By selecting this target, index outputs are representative of the medium- and long-term sediment transport processes where sediment accumulation and transport take place also in the channels (Murphy et al., 2019).

2.3 | Aggregated index of runoff and sediment connectivity

In a recent study, López-Vicente et al. (2020) evaluated the performance of four indices of SC to assess hillslope-channel and hillslope-outlet SC in three headwater sub-catchments located in La Sierra de Los Donceles, obtaining the best results with the AIC (López-Vicente & Ben-Salem, 2019), especially when the catchment outlet was used as computation target. AIC is a modified and extended version of the equation developed by Borselli et al. (2008), including some of the modifications proposed by Cavalli et al. (2013).

The index is composed by two modules, the downslope module (D_{dn}), which represents sediment and runoff probability of reaching a defined sink along the flow path. The upslope module (D_{up}) considers the potential descending routing of runoff taking place upslope and implements a 'stream power'-like approach. AIC is calculated following the next equations:

$$AIC_k = \log_{10} \left(\frac{D_{up,k}}{D_{dn,k}} \right) = \log_{10} \left(\frac{\overline{R_t} \cdot \overline{RT} \cdot \overline{C_t} \cdot \overline{K_p} \cdot \overline{S} \cdot \sqrt{\overline{A_k}}}{\sum_{k=i}^n \frac{d_i}{AWC_i}} \right) \quad (1)$$

$$AWC_i = R_{ti} \cdot RT_i \cdot C_{ti} \cdot K_{pi} \cdot S_i \quad (2)$$

where d_i is the flow path length downstream, AWC is the aggregated weighting factor at catchment scale, R_t is the normalized rainfall erosivity factor for the period t (values among 0–1), RT is the roughness of the terrain factor that reflects how the local changes on slope gradient can accelerate or slow down overland flow velocity (Grohmann et al., 2011) (normalized values range between 0 and 1), C_t is the RUSLE vegetation management factor for the period t (values range between 0 and 1), K_p is the soil permeability factor (normalized values range between 0 and 1) and S is the slope gradient factor ($m \cdot m^{-1}$).

To calculate the R_t factor, rainfall erosivity, El_{30t} was previously calculated at monthly scale as the sum of the erosivity of each rainfall event:

$$El_{30} = (E)(I_{30}) = \left(\sum_{k=1}^m e_r \Delta V_r \right) I_{30} \quad (3)$$

$$e_r = 0.29[1 - 0.72 \exp(-0.082i_r)] \quad (4)$$

$$i_r = \frac{\Delta V_r}{\Delta t_r} \quad (5)$$

where m (n) is the number of temporal intervals established for each rainfall event; e_r (in $MJ \cdot ha^{-1} \cdot mm^{-1}$) is the kinetic energy of a rainfall event for the r period (linked to the temporal resolution of the precipitation record at the weather station); ΔV_r (in millimetres) is the volume of rainfall during the r period; I_{30} (in $mm \cdot h^{-1}$) is the maximum rainfall intensity in 30 min of each event, I_r (in $mm \cdot h^{-1}$) is the rainfall intensity for the r period; and Δt_r (in minutes) is the r period duration.

The calculated El_{30t} values in Equation 3 which were lower than 0.01, were converted to $El_{30t} = 0.01$ to avoid computational errors. In this study, the duration of the t period in Equations 1 and 2 was equal to one average year, therefore, represented values are representative of the structural SC of the studied catchments.

Although the addition of the R_t factor is crucial to study functional SC, which can reflect real sediment transport dynamics, in this case of study, we considered the importance of determining structural SC. Due to the great rainfall-erosivity differences between scenarios – almost twice in the second scenario (see Table 3) –, having only a functional SC point of view could mislead the conclusions of the study, that is why, calculating structural SC maps could allow us to study the effect of the different post-fire measures under the same rainfall conditions or without considering the influence of rainfall. The R_t factor (Equation 3) was calculated based on the 'Cenajo' reservoir (Figure 1). This station is included in the weather station network of

TABLE 3 Changes of the mean input values of the studied scenarios and catchments

Scenario	Dates (duration)	DEM (LiDAR)	Rainfall (mm yr ⁻¹)	El ₃₀ (MJ mm ha ⁻¹ h ⁻¹ yr ⁻¹)	R _t (0–1)	C-RUSLE				
						C. Pos	C. Con	C. Gril	C. Pin	C. Ray
Pre-man	July 2012– June 2013	Year 2009	440	619.2	0.540845	0.11	0.11	0.11	0.13	0.07
Post-man	July 2014– June 2015	Year 2016	410	1145.0	1.000000	0.095	0.09	0.098	0.10	0.07

El₃₀, calculated value of rainfall erosivity; R_t, rainfall erosivity factor in the aggregated index of connectivity (AIC).

the Segura River basin (data source: CHSegura-SAIH; code 04A02P01) and it is close to the study area (Table 3).

For these reasons, apart from the usual AIC functional (AIC_F) approach, for the same previously explained scenarios (Pre-man and Post-man) and target (outlet), we calculated structural SC maps (AIC_S) keeping the R_t factor value equal to 1. As rainfall erosivity in the Post-man scenario was higher than in the Pre-man scenario, the R_t factor was equal to 1 in both the AIC_F and AIC_S maps in the most recent scenario. Therefore, we obtained three maps of SC, two for the Pre-man scenario and one for the Post-man scenario.

2.4 | Simulation inputs

For each temporal scenario, a $2\text{ m} \times 2\text{ m}$ DEM was generated, using two different LiDAR (light detection and ranging) point cloud data provided by the Spanish Nacional Centre of Geographic Information (IGN). The data had dates of 2009 (representative of the Pre-man scenario) and 2016 (representative of the Post-man scenario). The data were processed with LAsTools and ArcGIS© 10.5 software and pre-processing task included the removal of those points that do not correspond to ground rebounds (e.g., vegetation). Additionally, local depressions were removed from the generated DEMs using the Planchon and Darboux algorithm (available in SAGA© 2.1.2), to ensure the continuity of the flow path lines across the hillslopes and in the streams. A gradient of 0.01° was considered as the minimum gradient that would permit the flow cross the filled sinks. Once the DEMs were pre-processed, the flow accumulation maps were calculated, running the Deterministic Infinity (D-Inf or D_∞) algorithm, and used to define the boundaries of the different catchments.

With regard to the different AWC_i factors: The Slope gradient (S_i) was calculated using the ArcGIS© 10.5 slope tool and values (%) were expressed on a per unit bases. The S_i values lower than 0.005 must be adjusted to $S_i = 0.005$ and higher than 1 must be set to a maximum value of $S_i = 1$. The roughness of the terrain (RT_i) factor was calculated as the normalized and inverse values of the standard deviation of the slope gradient, which was estimated using the DEMs and the 'Residual Analysis (Grid)' tool of SAGA© 2.1.2. A minimum value of 0.001 of RT_i was considered in order to avoid calculus errors with the GIS (geographic information system) tools.

The map of the soil permeability (K_p) factor was obtained using the lithostratigraphic units map (1:50,000) provided by the Spanish Geological Institute (IGME) and did not change between the two

temporal scenarios. The 'moderate' permeability units took the higher K_p value ($K_p = 1$), while the 'high' and 'very high' permeability units took K_p values of 0.667 and 0.333, respectively.

As mentioned earlier, the R_t factor (Equation 3) of each temporal scenario was calculated using the records every 5 min of the 'Cenajo' reservoir weather station. As we only used one weather station, no spatial changes on EI_{30} were considered in this study, and thus, a unique R_t value was obtained for the whole study area at each temporal scenario.

The maps of the C_t factor were generated by using the SIOSE land cover map provided by the Spanish Geographical Institute (IGN). Two land cover maps were used, the first one corresponds to the year 2011 (pre-wildfire vegetation conditions) and the second one to 2014 (2 years after the wildfire) (Supporting Information Figures S1 and S2). The structure of each SIOSE polygon came as the result of the combination of the different covertures inside that polygon (tree crops, conifer forest, shrubs, etc.) with different percentages linked to each land use (e.g., 60% of conifer forest; 25% of dense shrubs; and 15% of herbs). If very accurate, the maps needed some additions such as trails and the steep banks of the gullies with bare soil. These features did not occupy a significant percentage of the total area, but they are relevant in terms of soil erosion and preferential flow pathways.

The C-factors (Supporting Information Table S1) were designated to the land uses of the two scenarios using the values proposed by Panagos et al. (2015). For the Pre-man scenario (immediately after the wildfire), we followed the approach of Martínez-Murillo and López-Vicente (2018), and multiplied the 2011 (pre-fire) C-RUSLE map with the weighted burn severity map, using the weighting values proposed by Yochum and Norman (2015): Low burn severity = 1.10, moderate burn severity = 2.25 and high burn severity = 3.75. Nevertheless, these ratios were modified to maintain a harmonized C value dataset within the same range established by Panagos et al. (2015) for recently burned areas (maximum C factor of 0.55).

The burn severity assessment was based on the dNBR values obtained by Gómez-Sánchez et al. (2017) for the same forest fire. These dNBR values were categorized following the classification of the USGS FIREMON programme (USGS, 2004) shown in Table 4. Unburned areas will have values close to zero showing small or null differences between scenarios, however, severely burned areas will show higher dNBR values.

The post-fire management measures were carefully mapped using the orthophotograph provided by the IGN (aerial photograph taken in 2015) as well as the geographic data provided by the local administration. They were introduced to the input maps as modifications of

TABLE 4 The scaled index of burn severity based on values derived from the USGS FIREMON programme (USGS, 2007) and the differenced normalized burn ratio (dNBR). The area (percentage) of each basin affected by the different fire severity classes is also included

dNBR value	Burn severity class	C. Pos (%)	C. Con (%)	C. Gri (%)	C. Pin (%)	C. Ray (%)
< -0.25	High post-fire regrowth	—	—	—	—	—
-0.25 to -0.10	Low post-fire regrowth	—	—	—	—	—
-0.10 to +0.10	Unburned	22.48	14.89	39.57	—	65.70
0.10 to 0.27	Low severity	0.68	1.15	0.45	0.08	0.21
0.27 to 0.44	Moderate-low severity	18.72	35.64	24.97	21.65	14.75
0.44 to 0.66	Moderate-high severity	53.41	20.77	31.12	76.62	19.12
>0.66	High severity	4.69	27.54	3.89	1.64	0.21

ND: No data.

some of the original input layers. In the Post-man scenario, the channel measures were introduced to the input index by using the information included in the DEM. Regarding hillslope measures, the C-factor map was modified for the Post-man scenario to include them. Log and contour felled log debris barriers were considered as elements with a higher flow impedance, and took a value depending on their efficiency retaining sediment fluxes. In a study area located in north-eastern Spain with similar conditions to ours where log barriers were also built after wildfire to control soil erosion and runoff, Badía et al. (2015) identified that these features had an efficiency retaining sediments of 83%. Contour felled log debris barriers, however, were considered to have a lower efficiency, based on the study carried out by Aristeidis and Vasiliki (2015) in burned Aleppo pine forests in Greece, under Mediterranean conditions only a 45% of the contour felled log debris barriers worked efficiently. These efficiencies were applied to the considered value of maximum flow impedance (0.001). Afforestation also modified the C-factor map; this modification was based on a yet unpublished study which is being carried out at this study area. The results of this study show that the cover difference between control plots and the reforested ones was of a 30.51% and 19.79% for the mechanical subsoiling and the manual digging afforestation, respectively. This value of cover difference was added to the shrub percentage of each SIOSE polygon where afforestation took place. Finally, the skid trails were also mapped, and its RUSLE C factor was similar to that of the other trails in the study area.

To set the outlet as the target of the simulation, the flow-direction map was modified. Those pixels located at the outlet of each basin were given a value of zero, generating a mask to modify the flow direction map. This computation setup only affected the AIC down-slope component (D_{dn}).

2.5 | Aggregated index of connectivity values normalization

AIC results heavily depend on the simulation target and input values and resolution, such as the catchment drainage area. In order to obtain comparable values between the different catchments – that are not linked among them during the index computation process – we normalized the AIC outputs of Equation 1 by using the following expression proposed by López-Vicente et al. (2021):

$$AIC_N = AIC_i \times \log_{10}(10 + \text{FlowLength}_{sim}) \quad (6)$$

where AIC_N is the normalized index of SC.

This adjustment was done for each basin separately, using its own flow path length (in metres) and considering its simulation target (outlet) as a reference. The previously modified flow direction map generated for the AIC_{OUT} target was used to calculate the flow length map.

2.6 | Statistical analysis and specific sediment yield field measurements

To assess how different were the temporal SC changes between those areas with hillslope barriers and non-treated, a one-way

analysis of variance (ANOVA) and *post hoc* Tukey test (95% of confidence) were calculated. To do so, the five catchments were divided in a total of 929 sub-catchments, 677 in the burned area (Figure S4). For the burned sub-catchments, hillslope barriers density (in $m \text{ ha}^{-1}$) was estimated, and three categories were established: no-treatment; barriers density $< 100 \text{ m ha}^{-1}$; barriers density $> 100 \text{ m ha}^{-1}$.

A different procedure was followed with afforestation areas. This measure was only implemented in one catchment (C. Pin), so instead of using the sub-catchment criteria, SC values were extracted from a total of 1200 random sample points within the reforested (subsoiled and dug) areas and similar control areas of C. Pin. The statistical analysis was also a one-way ANOVA and a *post hoc* Tukey test.

Regarding the sedimentological dynamic within the five catchments, and using independent values from index computation, we measured the accumulated sediment behind the 10 new concrete check-dams to estimate the sediment yield (SY) and area specific sediment yield (SSY). The annual rates of SY and SSY gave us an accurate measurement of the soil erosion dynamic at the sub-catchment scale and after the post-fire management practices were done. Despite the existence of 11 old concrete check-dams within the study area – built before the fire – we did not use them in this study owing to two reasons: (i) they do not offer a complete view of the sedimentological response of the five catchments because they are only located in three catchments (Table 2); and (ii) most of the hillslope (e.g., log erosion barriers, contour felled log debris) and channel (e.g., small rock check-dams) measures are not located in the drainage area of the old concrete check-dams, whereas the drainage area of the new concrete check-dams includes most of the small rock check-dams and hillslope measures (Figure 2). The location and characteristics of these check-dam areas are described in Table 5.

The surveys to measure SY were done during June–July 2019, following the sections method proposed by Díaz et al. (2014) using a total station (LEICA TC405) and a high performance GNSS device (LEICA GPS1200). This method was chosen due to its higher accuracy estimating the volume behind check-dams (Ramos-Diez et al., 2017). We also took six bulk density samples of each sediment wedge using a manual drill and a 50-cm³ cylinder, the samples were dry in an oven at 105°C and weighted. Then, SY (Mg yr^{-1}) and SSY ($\text{Mg ha}^{-1} \text{ yr}^{-1}$) were calculated as showed in Equations 7 and 8:

$$SY = \frac{SV \cdot BD_{SED}}{TE} \times 100 \quad (7)$$

$$SSY = \frac{SY}{A} \quad (8)$$

where SV (in m^3) is the accumulated sediment volume behind the check-dams; BD (in Mg m^{-3}) is the sediments bulk density; A (in hectares) is the drainage area; and TE (%) is the sediment trap efficiency of the check-dams (Quiñonero-Rubio et al., 2016).

Check-dams 3 and 5 were finally discarded from the analysis due to the difference between the area of their sub-catchments and the others, taking into account the influence that area has over the estimation of SSY (Bellin et al., 2011).

TABLE 5 Main characteristics of the check-dams in the five catchments

Basin	Check-dam	UTM X	UTM Y	Completion date	Upstream measures	Area (ha)	Height (m)	Width (m)	Volume (m ³)	BD (Mg m ⁻³)	TE (%)	SSY (Mg ha ⁻¹ yr ⁻¹)
C. Pos	1	610269	4252670	16 September 2013	HB, RC	143	6.25	38.35	304.53	1.018	30.9	1.20
C. Con	2	611678	4251797	30 July 2013	HB	194	6.40	38.75	585.70	1.002	38.8	1.31
C. Gri	3	614441	4251178	28 November 2013	—	9	6.70	26.00	160.47	1.178	78.9	4.76
C. Gri	4	614291	4250785	23 October 2013	HB, RC	87	4.90	21.00	209.53	1.172	33.7	1.48
C. Pin	5	613360	4249533	17 July 2013	AF	3	2.90	23.00	45.02	1.034	75.9	3.45
C. Pin	6	613389	4249534	4 July 2013	AF, HB, RC	34	5.80	38.00	163.58	1.027	50.3	1.64
C. Pin	7	613847	4249857	12 September 2013	RC	65	6.38	26.00	135.45	0.982	30.4	1.17
C. Pin	8	612545	4249847	31 October 2013	—	47	4.25	29.00	115.58	1.259	34.1	1.63
C. Ray	9	609399	4249982	6 November 2013	RC	66	6.45	36.00	389.52	1.047	55.3	1.96
C. Ray	10	608724	4250783	16 October 2013	RC	51	6.22	28.00	71.32	0.747	22.7	0.81

Upstream measures: HB, hillslope barriers; AF, afforestation; RC, rock check-dams; BD, bulk density; TE, trapping efficiency; SSY, specific sediment yield.

3 | RESULTS

3.1 | Estimated sediment connectivity at catchment scale – I: Structural and functional values

Meaningful differences between the two approaches (functional and structural) were clearly observed. The lowest AIC_{N-OUT} values were obtained for the $AIC_{N-OUT}F12$ (year 2012) with values between -40 and -21.4 considering all the study area (Figure 3), $AIC_{N-OUT}S12$ and $AIC_{N-OUT}14$ (year 2014) took values which varied between -40.1 to -20.9 and -21.5 to -39.8 , respectively. These differences between the two approaches persist when considering the mean AIC_{N-OUT} values of the burned area for each basin and temporal scenario (Table 6). Considering the functional approach, $AIC_{N-OUT}F$ mean values increased at the Post-man scenario in all the studied catchments ranging this increment between 4.45% for C. Ray and 5.89% for C. Gri. However, the $AIC_{N-OUT}S$ mean values were slightly lower at the Post-man scenario, with decreases between -0.85% for C. Gri and -1.86% for C. Ray.

When comparing the mean AIC_{N-OUT} values of the five studied catchments burned area, differences were also observed (Table 6). C. Pin was the basin with the highest mean AIC_{N-OUT} values, with -26.32 and -24.50 for $AIC_{N-OUT}F$ and the $AIC_{N-OUT}S$ of the Pre-man scenario, respectively, and -24.80 for the Post-man scenario. C. Ray also had mean AIC_{N-OUT} values above -30 for the different scenarios and approaches. C. Pos showed the lowest AIC_{N-OUT} mean values which varied between -31.96 and -30.05 for the functional and structural Pre-man scenario and -32.46 at the Post-man scenario. C. Con and C. Gri had intermediate mean values: -31.96 and -31.52 for $AIC_{N-OUT}F12$, -30.05 and -29.42 for $AIC_{N-OUT}S12$, and -30.40 and -29.67 for $AIC_{N-OUT}14$.

3.2 | Estimated sediment connectivity at catchment scale – II: Spatial patterns

Attending to the spatial patterns, the analysis was focused on the areas with the highest (percentile 90, P90) and lowest (percentile 10, P10) values of AIC_{OUT} (Figure 4). The highest values (P90) were recorded on those areas close to the outlet and in the channels ranging between 8% and 9% of the pixels of each basin. The lowest AIC_{OUT} values (P10) were recorded in upper areas that also account around 8–9% of the total pixels.

Regarding the functional approach, for the different temporal scenarios C. Ray and C. Con were the catchments with a higher percentage of P90 pixels with a 9.277% and 9.302% for the Pre-man scenario and 9.630% and 9.652% for the Post-man scenario. The lowest percentage of P90 pixels was recorded at C. Pin, with a 7.983% for the Pre-man scenario and 8.494% for the Post-man. C. Pin was also the basin with a lower percentage of P10 pixels with an 8.852% and an 8.428% for the Pre-man and the Post-man scenario in that order. At the other catchments, that percentage varied between 8% and 9% having C. Pos the higher percentage with 9.601% and 9.514%.

The structural approach results were similar, with slightly higher P90 percentages than the functional Pre-man scenario but still about 8–9%. The highest percentage of P90 pixels were also observed in C. Ray and with 9.642% and C. Con with 9.294%. C. Pin was again the

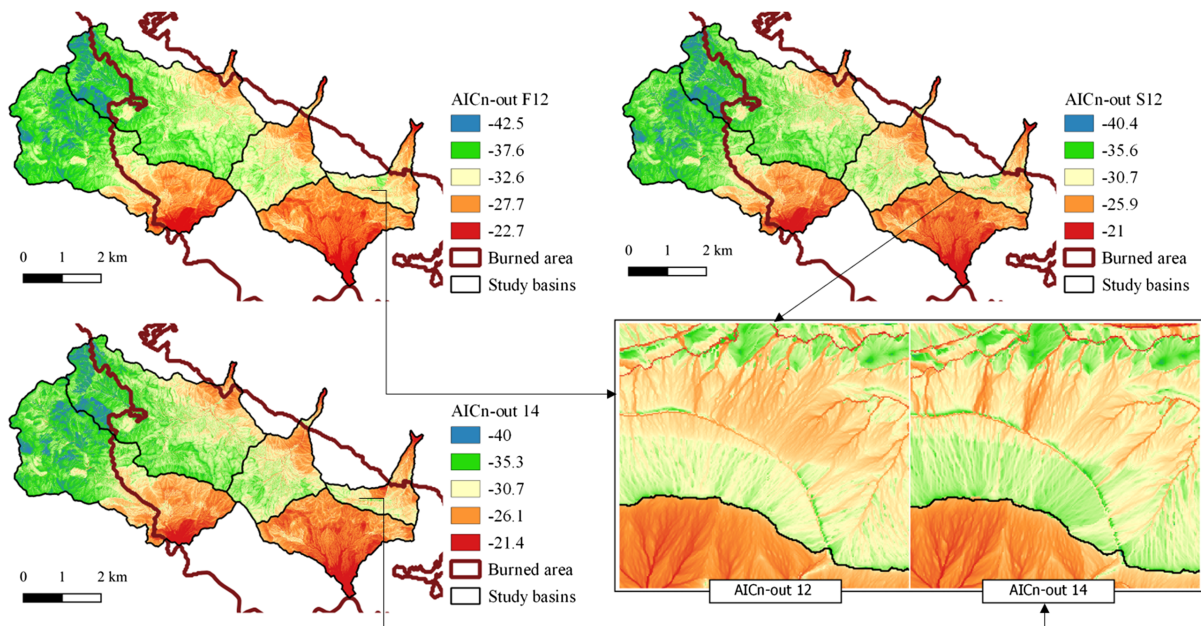


FIGURE 3 Maps of AIC_{N-OUT} of the pre-management scenario (2012) for the functional (F; left top map) and the structural (S; right top map) and the post-management scenario (2014; bottom map). In the left bottom of the figure an enlarged image of an area in C. Gri where the SC changes between temporal scenarios are visible [Color figure can be viewed at wileyonlinelibrary.com]

TABLE 6 Normalized sediment connectivity (SC) values targeting the catchments' outlet (AIC_{N-OUT}) and temporal changes (ΔAIC_{N-OUT} ; %) per catchment. For the functional (F) and structural (S) approaches and the pre-management (Pre-man) (12) and post-management (Post-man) (14) scenario. Only the burned area was considered

Basin	$AIC_{N-OUT}F12$	$AIC_{N-OUT}S12$	$AIC_{N-OUT}14$	$\Delta AIC_{N-OUT}F$	$\Delta AIC_{N-OUT}S$
C. Con	-31.96	-30.05	-30.40	4.90%	-1.14%
C. Gri	-31.52	-29.42	-29.67	5.89%	-0.85%
C. Pin	-26.32	-24.50	-24.80	5.79%	-1.21%
C. Pos	-34.37	-32.17	-32.46	5.56%	-0.89%
C. Ray	-28.50	-26.74	-27.23	4.45%	-1.86%

basin with the lower P90 pixels percentage with 8.029%. Concerning the low SC pixels (P10) the highest percentage was again observed in C. Pos with 9.576% and C. Con with 9.205%. With an 8.849% C. Ray was the one with the lower P10 pixels percentage.

As can be observed in Figure 4 the SC patterns of the different scenarios were very similar in all the catchments regardless of the SC approach (F: functional or S: structural). The overlap percentage of the P10 and P90 pixels between scenarios was around 99% with the only exception of C. Gri which had a lower overlapping percentage of 88%.

3.3 | Hillslope measures performance

With regard to hillslope barriers, meaningful differences on ΔAIC_N were observed between having different barrier densities or not (Figure 5). These differences appear for both functional and structural approaches.

From a functional approach, all the sub-catchments, independently of their treatment, suffered a SC increase at the Post-man scenario. Non-treated sub-catchments (NB) had the highest mean SC increase for $\Delta AIC_{N-OUT}F$ with a 6.083%. Those sub-catchments with a low density of barriers ($< 100 \text{ m ha}^{-1}$) experienced a similar change

between scenarios than then-treated ones with a mean value of $\Delta AIC_{N-OUT}F = 5.778\%$. Whereas sub-catchments with a higher density of built barriers ($> 100 \text{ m ha}^{-1}$) had the lowest increment with $\Delta AIC_{N-OUT}F = 4.966\%$. However, from a structural SC approach, a decrease on mean SC between temporal scenarios can be observed. In NB sub-catchments, SC had a decrease of $\Delta AIC_{N-OUT}S = -0.017\%$. Sub-catchments with low barriers density had similar mean values again with $\Delta AIC_{N-OUT}S = -0.193\%$. The greatest mean SC decrease took place again in the sub-catchments with a higher density of barriers, with $\Delta AIC_{N-OUT}S = -0.879\%$.

According to the ANOVA and Tukey tests results, those sub-catchments with a higher density of hillslope barriers ($> 100 \text{ m ha}^{-1}$) had significantly lower $\Delta AIC_{N-OUT}F$, and $\Delta AIC_{N-OUT}S$, values than the NB catchments or those with a low density of hillslope barriers ($< 100 \text{ m ha}^{-1}$) (Figure 5). Only for $\Delta AIC_{N-OUT}F$, low density sub-catchments ($< 100 \text{ m ha}^{-1}$) resulted to be significantly different to non-treated sub-catchments. No significant differences were observed between NB and low-density sub-catchments for $\Delta AIC_{N-OUT}S$.

Afforestation also had a meaningful impact on SC changes between the two temporal scenarios. Treated areas had always a lower SC than untreated (NT), mirroring the spatial pattern of the C factor in the Post-man scenario (Figure 5). NT areas had a mean SC

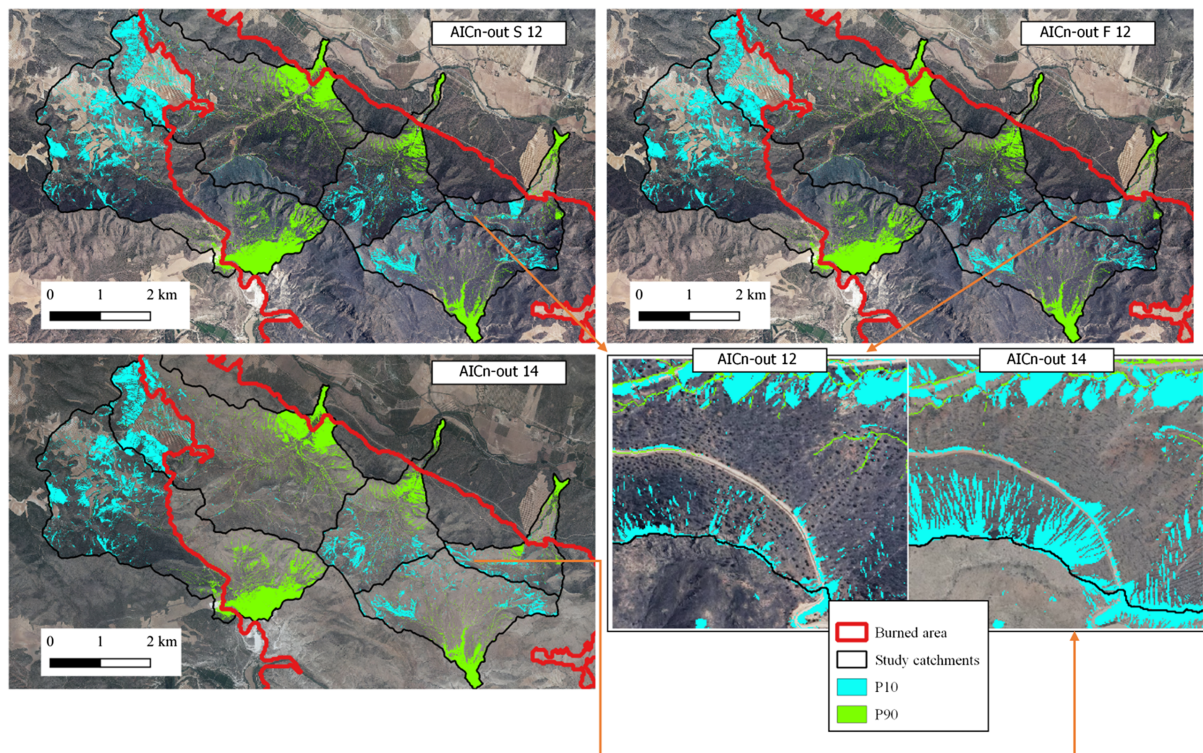


FIGURE 4 Maps showing the areas with the highest (percentile 90) and lowest (percentile 10) values of estimated sediment connectivity and the location of the existent check-dams in the area for the different temporal scenarios and the functional (F) and structural (S) approaches. In the left bottom of the figure an enlarged image of an area in C. Gri where the SC changes between temporal scenarios are visible [Color figure can be viewed at wileyonlinelibrary.com]

increase $\Delta AIC_{N-OUTF} = 4.83\%$ between temporal scenarios. Reforested areas with the digging soil preparation (D), had a similar $\Delta AIC_{N-OUTF} = 4.81\%$. Moreover, subsoiled areas (SS) had lower SC increases ($\Delta AIC_{N-OUTF} = 3.67\%$). From the structural point of view, NT areas had a mean SC decrease of $\Delta AIC_{N-OUTS} = -1.44\%$. D-areas showed values of $\Delta AIC_{N-OUTS} = -7.94\%$ and SS had the greatest mean decrease with $\Delta AIC_{N-OUTS} = -3.06\%$.

As stated in the ANOVA and Tukey HSD tests results, it can be observed that SS areas had significantly lower ΔAIC_{N-OUTF} or ΔAIC_{N-OUTS} than NT- and D-areas, moreover, no significant differences were found between D and NT.

3.4 | Channel measures performance

The expected disconnectivity of upstream areas produced by RC and CC on the SC maps was not noticeable at the AIC_{N-OUT} maps; this shortcoming can be observed in Figure 6. No disconnectivity at the flux throughout the channels where the structures were built or in the upstream areas can be observed in this area of C. Pin (check-dam no. 7) with high density of RC in the channels upstream the CC.

3.5 | Sediment connectivity linked to the specific sediment yield

The relationship between the SC changes between temporal scenarios and the measured SSY for the selected CC was positive (Figure 7), with a coefficient of determination (R^2) for ΔAIC_{N-OUTF} and ΔAIC_{N-OUTS} with a Pearson R^2 of 0.677 and 0.752, respectively.

Those CC sub-catchments where hillslope and channel measures were carried out with a low density or absent were also the sub-catchments with the higher SSY (nos 6, 8 and 9). However, those CC sub-catchments with channel and hillslope measures built in a higher density resulted in a lower SSY value (nos 1, 2, 4, 7 and 10). Those sub-catchments with a higher density of measures upstream were also the ones which had a lower AIC_{N-OUTF} increase and a higher AIC_{N-OUTS} increase between the temporal scenarios.

4 | DISCUSSION

4.1 | Catchment response

In previous studies carried out in three sub-catchments of the same study area, we observed that AIC_i can be more sensible than other SC indices to temporal changes in burned areas (López-Vicente et al., 2020). In this study, we were aiming to assess SC at catchment scale and study the effect of post-fire management strategies on it. After normalization, differences among catchments, if comparable, were still observed. The catchment with a higher elongation ratio (C. Pin), was the one with the highest AIC_{N-OUT} mean value, that speaks about the great influence of the catchment morphometry on SC. The location of the outlet, although reduced by the previous normalization of the results still had a strong influence on SC. Catchments as C. Ray, despite having a lower elongation ratio, had steeper slopes close to the outlet which was traduced in higher mean AIC_{N-OUT} values. However, other catchments like C. Con with a higher elongation ratio and stream density had lower values due to the location of the outlet. Slope was other of the more influential

FIGURE 5 Relationship between the temporal changes of estimated sediment connectivity (ΔAIC_{N-OUT} ; %) and barriers density (NB: no barriers. 0–100 ($m\ ha^{-1}$), >100 ($m\ ha^{-1}$)) and afforestation treatment (SS, subsoiled; NT, no treatment; D, dug). Those boxplots with different capital letters had significant differences according to the *post hoc* Tukey test results [Color figure can be viewed at wileyonlinelibrary.com]

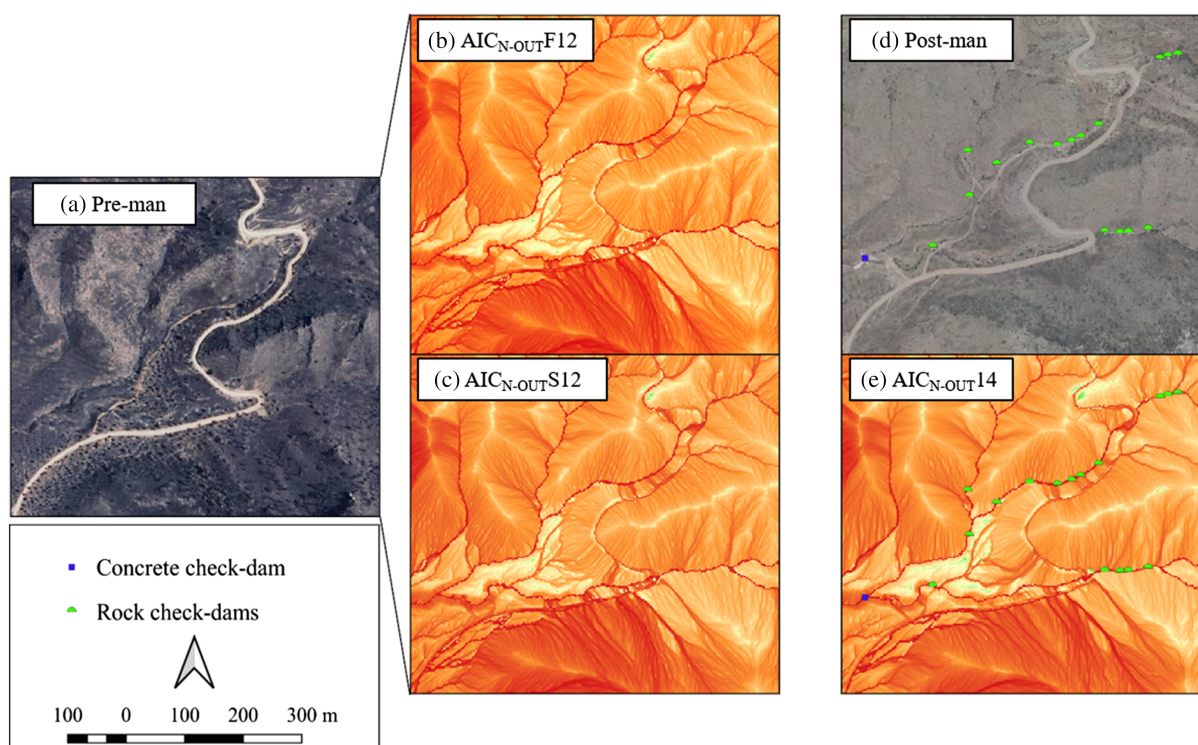
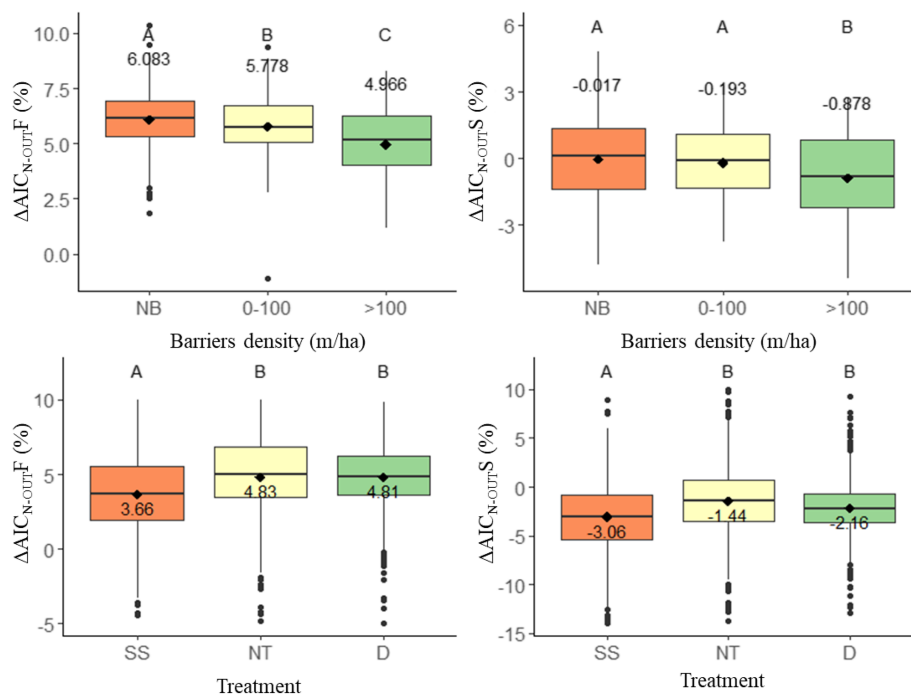


FIGURE 6 Local effect of check-dams on AIC_{N-OUT} at the sub-catchment no. 7 (C. Pin): (a) aerial image of the area at the Pre-man scenario without any measures; (b) $AIC_{N-OUT} F_{12}$ map for the Pre-man scenario and the functional approach; (c) $AIC_{N-OUT} S_{12}$ map for the Pre-man scenario and the structural approach; (d) aerial image of the area at the Post-man scenario with RC and CC; (e) $AIC_{N-OUT} I_{14}$ map for the Post-man scenario and the functional and structural approaches [Color figure can be viewed at wileyonlinelibrary.com]

factors on SC, those areas with higher slopes were highly connected, this can be also observed in the percentile studio.

Regarding the combined effects of the post-fire mitigation measures to the mean values of each catchment, catchments C. Pin and C. Con, which had a high density of post-fire mitigation measures experienced the highest structural decrease and the lowest functional SC increase. Also C. Ray which had high density of measures located close to the outlet of the catchment resulted in a higher decrease of

$AIC_{N-OUT} S$ and a lower decrease of $AIC_{N-OUT} F$. Percentile maps showed that lower SC areas (P10) were located in upper areas, in some cases unburned areas with soft slopes and agricultural land. However, the majority of P90 pixels were at the outlets, the channel, and very steep areas close to the outlets. These spatial patterns slightly changed between $AIC_{N-OUT} F$ and $AIC_{N-OUT} S$ which reveals that no structural changes were produced when including rainfall erosivity as a factor in the computation. Those spatial patterns were also

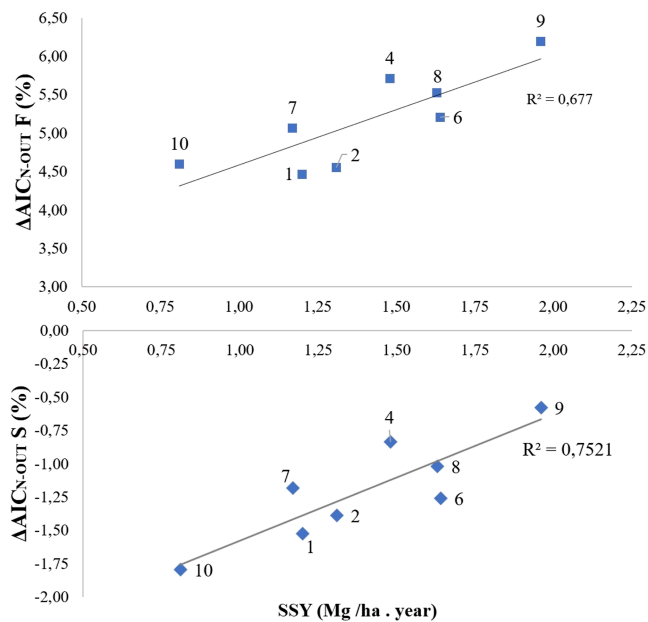


FIGURE 7 Relationship between the temporal changes of estimated sediment connectivity (ΔAIC_{N-OUT} ; %) at each check-dam sub-catchment and the measured values of area specific sediment yield (SSY; $Mg\ ha^{-1}\ yr^{-1}$) in the check-dam [Color figure can be viewed at wileyonlinelibrary.com]

similar when comparing the two temporal scenarios, which reveals that no important structural changes were observed between them despite the undertaken post-fire management practices.

4.2 | Relevance of computing structural and functional SC

With regard to the differences between temporal scenarios, it can be seen that depending on the SC approach (structural or functional) AIC_{N-OUT} values increased at the Post-man scenario, which is explained by the difference between rainfall erosivity in the two scenarios. From a structural approach, the incipient vegetation recovery, and the undertaken measures, reduce SC with respect to the Pre-man scenario, however, precipitation plays a key role in hydrological processes as one of the main drivers of runoff generation. These results highlight the importance of including factors which enable us to reflect functional SC to overcome the limitations of the structural approach. Structural SC is by definition static (Turnbull & Wainwright, 2019), functional SC implies dynamic processes such as rainfall which vary among the temporal scale. The use of more 'complete' indices such as AIC_N have enabled the evaluation of the potential vulnerability of fired affected catchments and the performance of post-fire management strategies (which alter the structure of the system) according to more variable factors.

4.3 | Hillslope measures performance

4.3.1 | Hillslope barriers

The use of hillslope barriers produced a significant reduction of SC with respect to the catchment outlet when the density was higher

than $100\ m\ ha^{-1}$. The differences between high density and low-density sub-catchments were also significant, revealing that only when applying a certain density of barriers, the ground cover is enough to reduce SC effectively. Authors like Robichaud et al. (2010) recommend to combine these hillslope barriers with other treatments – like mulching – to increase the ground cover and reduce sediment losses. In the same study area, Gómez-Sánchez et al. (2019) observed that hillslope barriers (if built in a proper way) trapped sediments efficiently and influence several soil variables improving edaphic conditions. However, they also pointed that their application in post-fire restoration plans, which is commonly applied in steep areas, is usually conditioned by the lack of vegetal material to build them or by the hazards of working in those areas.

Our results show that when the density of barriers was low, no difference was found between those sub-catchments and untreated ones. That is explained by the small area of influence of these barriers, which is reduced to the siltation wedge behind each barrier, which makes that low-density areas perform in a less effective than higher density ones. Nevertheless, it must be highlighted that these low-density sub-catchments were usually south facing and steep ones, where, as mentioned earlier, the lack of suitable trees to build barriers makes impossible to build them in high densities.

4.3.2 | Afforestation

Vegetation alters SC and reduce erosion and increase deposition in the hillslopes by increasing roughness and increasing the strength of the substrate by the action of the roots (Sandercock & Hooke, 2011). Regarding the effect of the different afforestation techniques to AIC_{N-OUT} , only SS areas significantly decreased SC with respect to NT. This method is being used because is clearly cheaper than D. Barberá et al. (2005), who studied the short and intermediate-term effects of afforestation soil preparation techniques in Mediterranean environments, observed that SS plots had a higher rate of survival than D; however, they also pointed that SS impact is higher due to the breaking of the petrocalcic horizon, and maintain that even with a higher cost and lower success rate, D must be considered. In our case, it is obvious that independently of the site preparation method, increasing ground cover will reduce SC and retain a higher amount of sediment in the hillslopes.

Despite the applied hillslope treatment, when considering a functional approach SC increased at the Post-man scenario. This fact can be explained by the higher erosive power of the rain in this temporal scenario. Further research must be conducted to study the rainfall threshold from which the applied hillslope measures do not reduce SC anymore. This fact shows the importance of including to SC indexes rainfall erosivity data which is one of the main trigger factors of soil erosion and sediment transport (travel distance and storage).

Being able to reflect on the effect of these hillslope treatments in structural SC using AIC_{N-OUT} or other SC indices is important, so it tells how disconnected the treated hillslopes from the outlet are (rivers draining into reservoirs and agricultural land in our case) under normal rainfall conditions. However, an extra value of AIC_N is that this index introduces a functional approach, which could allow managers to assess the catchment response and the undertaken measures under changing rainfall conditions. This information may be useful to

prioritize between different treatments depending on the restoration objective. It might be also of high interest to study if that SC reduction observed when targeting the catchment outlets, increases when AIC is focused in studying hillslope-stream connectivity (Lateral SC) which can be achieved by modifying the flow direction input raster to set the streams as targets.

4.4 | Channel measures performance and disconnectivity

Among channel measures, as mentioned earlier, CC did have a certain effect on SC, upstream the non-silted structures, the siltation wedge was detected by the model, although the check-dam was not detected, which did not result on the flow getting disconnected. The RC did not result in any significant changes of AIC_{N-OUT} . The utilized 2 m resolution DEM became a limitation to reflect the field-observed effect (disconnectivity) of channel measures on SC. Authors like Bombino et al. (2020), who assessed SC changes due to check-dams by modifying the index developed by Quiñonero-Rubio et al. (2013), had similar problems. Their index was unable to reflect that effect due to the lack of pixels covering the areas under the influence of the check-dams. On the contrary, Cucchiaro et al. (2019) successfully evaluated the role of check-dams in a debris-flow channel between temporal scenarios using the IC index (Cavalli et al., 2013), and observed that the built check-dams considerably decreased not only longitudinal SC (along the main channel) but also lateral SC (hillslope-to-channel). These authors were using a 1 m LiDAR-derived DEM, which in our case, was considered the best resolution over the 2 m one. This option was finally discarded because of the poor quality of the generated DEM in several patches where the point density of the available cloud was lower. Moreover, even though the problem with the structures of greater dimensions (CC) may be solved using this resolution, the effects of the numerous small structures (RC) would be still missing. To be able to properly detect these structures and the discontinuity that they produce in secondary channels a higher resolution than 1 m may be needed. However, we considered that this shortcoming only had a minor effect on the sedimentological evaluation of the catchments because of the limited amount of sediment retained by the smaller channel measures.

The DEM resolution must be chosen according to the study objective (Claessens et al., 2005), sometimes very accurate DEMs can weaken the correlations between the variable of interest and the topographic index (Sørensen & Seibert, 2007). In our case, to evaluate flow processes and sediment transport dynamics at the catchment scale very high resolutions are not needed, Thomas et al. (2017) pointed out that resolutions of 1 to 2 m were optimal for catchment scale modelling. Using extremely accurate pixel size, will allow to incorporate check-dams to the DEM in a precise mode, but at the catchment scale it may involve a great amount of data and calculation time. Furthermore, high resolution models (0.25 m) have been reported to not add many extra information with respect to 1 m ones (Cantreul et al., 2018).

Alternative solutions like those undertaken by Marchi et al. (2019) may be the best solution to the observed problem. These authors directly modified the pre-control-works DEM in those areas where control works were carried out, to recreate check-dams before

and after being silted. Additionally, they combined the LiDAR data with a terrestrial laser scanner survey to improve the resolution in the areas close to the check-dams. Doing it that way, they observed that check-dam construction produced an abrupt decoupling between upper and lower parts of the catchment, which disappear after the sediment filled up the check-dams.

Regardless of the followed method, in the present study area, being able to reflect the effect of check-dams on AIC_{N-OUT} with respect to the outlet of the catchment, it is also important to evaluate their location in consonance of the old ones. The presence of previous check-dams that are partially silted, may lead into already disconnected catchments and the investment of large amounts of money in these channel measures could be avoided.

4.5 | Sediment connectivity linked to the specific sediment yield

Measured SSY rates were low ($< 2 \text{ t ha}^{-1} \text{ yr}^{-1}$), but these results concur with those of SSY obtained in other studies which took place in the southeast of Spain (Romero-Díaz et al., 2007; Sougnez et al., 2011). The inclusion of the SSY allowed us to evaluate the actual spatio-temporal sediment dynamics within the check-dams' sub-catchments and compare it with the SC changes between scenarios, nevertheless this data must be considered carefully due to the construction date of the check-dams, which were not built till 1 year after the fire. Moreover, sediment delivery, and its associated ratio (sediment delivery ratio, SDR), is a complex process that presents significant changes over time in the same place, and between distinct places at the same moment: material stored as valley alluvium must leave the catchment during episodes of intensive erosion (Parsons et al., 2006). The positive correlation with a relatively high Pearson coefficient for the two approaches, indicate the ability of AIC_N and SC assessment, to represent the erosion potential at a catchment scale and the link between structural SC changes and erosion and deposition processes. This positive correlation between SC was also observed by Cucchiaro et al. (2019) in the Italian Alps. Using IC, they observed that deposition patterns had a strong correspondence with those areas where IC values decreased, and erosion processes prevailed where IC values increased.

The sub-catchments with lower SSY were also those with a higher density of hillslope and channel measures upstream of the concrete check-dam, which were in some grade those with a lower increase (functional approach) or a higher decrease (structural approach) of SC between temporal scenarios. Nevertheless, as the pre-fire and just after the fire (before post-fire practices) sediment dynamics are unknown in the same drainage of the 10 new concrete check-dams, the background differences between the measured sub-catchments are lacking. That can be a shortcoming of our approach as other factors could be influencing the SSY apart from the SC changes produced by forest fire and post-fire management.

4.6 | Post-fire management implications

The study of sediment connectivity is an important step to describe sediment dynamics at catchment scale and has a direct relation with

hazard assessment (Crema & Cavalli, 2018). The application of AIC to assess SC at catchment scale as a post-fire management tool should be considered, since it can help the planning and design of structural measures to prevent soil erosion and other hazards. Supporting managers with a tool which has a lower data requirement than other complex physically-based models (Cucchiari et al., 2019) and allows them not only to plan the location of the different measures after the fire but also to evaluate the effect of the carried measures might be differential in the future.

The significant reduction of AIC_{N-OUT} values produced by hill-slope measures as well as their positive local effects and the low environmental and landscape impact may encourage the use of these kinds of actuations over big check-dams which must be placed only when needed in strategic locations to protect downstream infrastructures.

Nevertheless, further research must be done to overcome the problems detected in this study. As it is shown in this study reflecting the effect of post-fire check-dams on SC is also a key issue to properly locate and evaluate the suitability of these structures. However, an optimal solution to the DEM resolution problem might be founded to make AIC_{N-OUT} able to detect the disconnectivity produced by the check-dams.

Other issues related with the improvement of the inputs and their ability to reflect the changes produced by wildfires must be addressed to differentiate even more AIC from other similar and SC indices like IC which require less inputs. One of the factors of AIC which still can be calculated in a much better way is the K factor, as forest fires not only remove vegetation but also affect soil physicochemical properties (Hedo et al., 2015). Factors like soil water repellency are proved to change drastically after fire affection and change soil permeability, becoming a key factor in runoff generation and sediment transport after forest fires (Stavi, 2019). This factor though, is not easy to extrapolate from the hillslope/plot scale to the catchment scale due to its complexity, nonetheless, it seems interesting to study how to incorporate it in to the aggregated W factor of this index.

5 | CONCLUSIONS

Studying the incidence of post-fire management practices on SC is a crucial issue to achieve an optimal planification of the works and to prevent possible hazards. In this study, we assessed SC at the catchment and sub-catchment scales and evaluated the effect of these practices on them with different results. The computation of post-fire SC before and after post-fire practices using AIC_{N-OUT} was satisfactory and the spatial distribution of SC values over the temporal scenarios was coherent with the observed sediment transport dynamics at sub-catchment scale (expressed as area-specific sediment yield - SSY). Approaching the modelling with a structural and a functional prism is also a key issue that can be drawn from this study. Although spatial patterns in both scenarios were similar regardless of the approach, incorporating the rainfall factor supposed an increase of SC in the Post-man scenario independently of management practices or vegetation recovery.

AIC was effective in reflecting hillslope measures effect. Hillslope barriers resulted in a certain disconnectivity, but their localized action significantly reduced their effect when they were

built in low densities. Also, afforestation supposed a reduction of SC by incrementing the soil cover. Further research about their efficiency must be done, nevertheless, both treatments may be considered in combination with others to achieve the aimed restoration goals. However, the resolution of the employed DEMs was not enough to reflect the effect of small-size channel measures on SC which was one of the main objectives of this article. In this respect, an optimal resolution or other ways to introduce their effect in the model seems crucial and opens an important investigation field for the future. The positive correlation between SSY and SC changes observed in this study makes AIC a very interesting tool for post-fire management, which will be also perfectly able to evaluate the effect of the different channel measures once the resolution problem is solved. The application of AIC to assess SC at catchment scale as a post-fire management tool should be considered and further research must be directed to improve the inputs quality to make it a more powerful tool.

ACKNOWLEDGEMENTS

The authors thank the Regional Government of Castilla-La Mancha (Junta de Comunidades de Castilla-La Mancha) for supporting the study and providing information about the undertaken measures in the burned area. This study was supported by funds provided to the VIS4FIRE Spanish R&D project (RTA2017-00042-C05-00) co-funded by the "Instituto Nacional de Investigación y Tecnología Agraria" (INIA) and FEDER programme. This study was done in the frame of the European Cooperation in Science and Technology (COST) action CA18135 'FIRElinks' (Fire in the Earth System: Science & Society). J. González-Romero holds a scholarship (Sbply/16/180501/000109) from the Regional Government of Castilla-La Mancha/European Social Fund (ESF, EU). The authors declare no conflict of interest.

DATA AVAILABILITY STATEMENT

The data that support the findings of this study are available from the corresponding author upon reasonable request.

ORCID

Javier González-Romero  <https://orcid.org/0000-0002-0065-5838>

Manuel Esteban Lucas-Borja  <https://orcid.org/0000-0001-6270-8408>

REFERENCES

- Albert-Belda, E., Bermejo-Fernández, A., Cerdà, A. & Taguas, E.V. (2019) The use of easy-barriers to control soil and water losses in fire-affected land in Quesada, Andalusia, Spain. *Science of the Total Environment*, 690, 480–491. <https://doi.org/10.1016/j.scitotenv.2019.06.303>
- Aristeidis, K. & Vasiliki, K. (2015) Evaluation of the post-fire erosion and flood control works in the area of Cassandra (Chalkidiki, North Greece). *Journal of Forestry Research*, 26(1), 209–217. <https://doi.org/10.1007/s11676-014-0005-9>
- Badía, D., Sánchez, C., Aznar, J.M. & Martí, C. (2015) Post-fire hillslope log debris dams for runoff and erosion mitigation in the semiarid Ebro Basin. *Geoderma*, 237–238, 298–307. <https://doi.org/10.1016/j.geoderma.2014.09.004>
- Barberá, G.G., Martínez-Fernández, F., Álvarez-Rogel, J., Albadalejo, J. & Castillo, V. (2005) Short- and intermediate-term effects of site and plant preparation techniques on reforestation of a Mediterranean semiarid ecosystem with *Pinus halepensis* Mill. *New Forests*, 29(2), 177–198. <https://doi.org/10.1007/s11056-005-0248-6>

- Bellin, N., Vanacker, V., van Wesemael, B., Solé-Benet, A. & Bakker, M.M. (2011) Natural and anthropogenic controls on soil erosion in the Internal Betic Cordillera (southeast Spain). *CATENA*, 87(2), 190–200. <https://doi.org/10.1016/j.catena.2011.05.022>
- Boix-Fayos, C., de Vente, J., Martínez-Mena, M., Barberá, G.G. & Castillo, V. (2008) The impact of land use change and check-dams on catchment sediment yield. *Hydrological Processes*, 22(25), 4922–4935. <https://doi.org/10.1002/hyp.7115>
- Bombino, G., Agostino, D.D., Labate, A., Boix-Fayos, C., Cataldo, M.F., Denisi, P. & Zema, D.A. (2020) A modified Catchment Connectivity Index for applications in semi-arid torrents of the Mediterranean environment. *River Research and Applications*, 36(5), 735–748. <https://doi.org/10.1002/rra.3606>
- Borselli, L., Cassi, P. & Torri, D. (2008) Prolegomena to sediment and flow connectivity in the landscape: A GIS and field numerical assessment. *Catena*, 75(3), 268–277. <https://doi.org/10.1016/j.catena.2008.07.006>
- Burguet, M., Taguas, E.V. & Gómez, J.A. (2017) Exploring calibration strategies of the SEDD model in two olive orchard catchments. *Geomorphology*, 290, 17–28. <https://doi.org/10.1016/j.geomorph.2017.03.034>
- C. P. B. (1977) Soil Taxonomy. A Basic System of Soil Classification for Making and Interpreting Soil Surveys. 1975. 754 pp., 12 coloured plates. Agriculture Handbook No. 436. Soil Conservation Service, U.S. Department of Agriculture. From Superintendent of Documents, U.S. Government Printing Office, Washington, D.C. 20402. Price \$17.50. - F. D. Hole 1976. Soils of Wisconsin. xvi + 223 pp., 8 pls, 151 figs, 26 tables. University of Wisconsin Press, Madison. Price \$15.00. ISBN 0 299 06830 7. *Geological Magazine*, 114(6), 492–493. <https://doi.org/10.1017/s0016756800045489>
- Calsamiglia, A., García-Comendador, J., Fortesa, J., López-Tarazón, J.A., Crema, S., Cavalli, M. et al. (2018) Effects of agricultural drainage systems on sediment connectivity in a small Mediterranean lowland catchment. *Geomorphology*, 318, 162–171. <https://doi.org/10.1016/j.geomorph.2018.06.011>
- Calsamiglia, A., Lucas-Borja, M.E., Fortesa, J., García-Comendador, J. & Estrany, J. (2017) Changes in soil quality and hydrological connectivity caused by the abandonment of terraces in a Mediterranean burned catchment. *Forests*, 8(9), 1–20. <https://doi.org/10.3390/f8090333>
- Cantreul, V., Bielders, C., Calsamiglia, A., Degré, A., Tech, G.A. & Déportés, P. (2018) How pixel size affects a sediment connectivity index in central Belgium. *Earth Surface Processes and Landforms*, 43(4), 884–893. <https://doi.org/10.1002/esp.4295>
- Cavalli, M., Trevisani, S., Comiti, F. & Marchi, L. (2013) Geomorphometric assessment of spatial sediment connectivity in small Alpine catchments. *Geomorphology*, 188, 31–41. <https://doi.org/10.1016/j.geomorph.2012.05.007>
- Cerdá, A. & Doerr, S.H. (2005) Influence of vegetation recovery on soil hydrology and erodibility following fire: an 11-year investigation. *International Journal of Wildland Fire*, 14(4), 423–437. <https://doi.org/10.1071/WF05044>
- Cerdá, A. & Robichaud, P. (2009) *Fire effects on soils and restoration strategies*, Vol. 5. Boca Raton, FL: CRC Press.
- Chartin, C., Evrard, O., Patrick-Laceyby, J., Onda, Y., Ottlé, C., Lefèvre, I. & Cerdan, O. (2017) The impact of typhoons on sediment connectivity: lessons learnt from contaminated coastal catchments of the Fukushima Prefecture (Japan). *Earth Surface Processes and Landforms*, 42(2), 306–317. <https://doi.org/10.1002/esp.4056>
- Chen, W. & Thomas, K. (2020) Revised SEDD (RSEDD) model for sediment delivery processes at the basin scale. *Sustainability*, 12(12), 4928. <https://doi.org/10.3390/su12124928>
- Claessens, L., Heuvelink, G., Schoolt, J.M. & Veldkamp, A. (2005) DEM resolution effects on shallow landslide hazard. *Earth Surface Processes and Landforms*, 30(4), 461–477. <https://doi.org/10.1002/esp.1155>
- Crema, S. & Cavalli, M. (2018) SedInConnect: A stand-alone, free and open source tool for the assessment of sediment connectivity. *Computers & Geosciences*, 111, 39–45. <https://doi.org/10.1016/j.cageo.2017.10.009>
- Cucchiaro, S., Cazorzi, F., Marchi, L., Crema, S., Beinat, A. & Cavalli, M. (2019) Multi-temporal analysis of the role of check dams in a debris-flow channel: Linking structural and functional connectivity. *Geomorphology*, 345, 106844. <https://doi.org/10.1016/j.geomorph.2019.106844>
- Díaz, V., Mongil, J. & Navarro, J. (2014) Proposal of a new methodology to assess the effectiveness of check-dams [Propuesta de una nueva metodología para determinar la efectividad de los diques en la retención de sedimentos]. *Cuadernos de Investigación Geográfica*, 40(1), 169–190. <https://doi.org/10.18172/cig.2531>
- Fernández, C., Fernández-Alonso, J.M. & Vega, J.A. (2020) Exploring the effect of hydrological connectivity and soil burn severity on sediment yield after wildfire and mulching. *Land Degradation & Development*, 31(13), 1611–1621. <https://doi.org/10.1002/ldr.3539>
- Fernández, C. & Vega, J.A. (2016) Effects of mulching and post-fire salvage logging on soil erosion and vegetative regrowth in NW Spain. *Forest Ecology and Management*, 375, 46–54. <https://doi.org/10.1016/j.foreco.2016.05.024>
- Fernández, C., Vega, J.A., Fonturbel, T., Barreiro, A., Lombao, A., Gómez-Rey, M.X. et al. (2016) Effects of straw mulching on initial post-fire vegetation recovery. *Ecological Engineering*, 95, 138–142. <https://doi.org/10.1016/j.ecoleng.2016.06.046>
- Foster, A.C., Armstrong, A.H., Shuman, J.K., Shugart, H.H., Rogers, B.M., Mack, M.C. et al. (2019) Importance of tree- and species-level interactions with wild fire, climate, and soils in interior Alaska: Implications for forest change under a warming climate. *Ecological Modelling*, 409, 108765. <https://doi.org/10.1016/j.ecolmodel.2019.108765>
- Frankl, A., Prêtre, V., Nyssen, J. & Salvador, P. (2018) The success of recent land management efforts to reduce soil erosion in northern France. *Geomorphology*, 303, 84–93. <https://doi.org/10.1016/j.geomorph.2017.11.018>
- Fressard, M. & Cossart, E. (2019) A graph theory tool for assessing structural sediment connectivity: Development and application in the Mercuray vineyards (France). *Science of the Total Environment*, 651, 2566–2584. <https://doi.org/10.1016/j.scitotenv.2018.10.158>
- Gómez-Sánchez, E., De las Heras, J., Lucas-Borja, M. & Moya, D. (2017) Assessing fire severity in semi-arid environments: application in Donceles 2012 wildfire (SE Spain). *Revista de Teledetección*, 49(49), 103–113. <https://doi.org/10.4995/raet.2017.7121>
- Gómez-Sánchez, E., Lucas-Borja, M.E., Plaza-Álvarez, P.A., González-Romero, J. & Sagra, J. (2019) Effects of post-fire hillslope stabilisation techniques on chemical, physico-chemical and microbiological soil properties in Mediterranean forest ecosystems. *Journal of Environmental Management*, 246, 229–238. <https://doi.org/10.1016/j.jenvman.2019.05.150>
- Grohmann, C.H., Smith, M.J. & Riccomini, C. (2011) Multiscale analysis of topographic surface roughness in the Midland Valley, Scotland. *IEEE Transactions on Geoscience and Remote Sensing*, 49(4), 1200–1213. <https://doi.org/10.1109/TGRS.2010.2053546>
- Heckmann, T., Cavalli, M., Cerdan, O., Foerster, S., Javaux, M., Lode, E. et al. (2018) Indices of sediment connectivity: opportunities, challenges and limitations. *Earth-Science Reviews*, 187, 77–108. <https://doi.org/10.1016/j.earscirev.2018.08.004>
- Heckmann, T. & Vericat, D. (2018) Computing spatially distributed sediment delivery ratios: Inferring functional sediment connectivity from repeat high-resolution digital elevation models. *Earth Surface Processes and Landforms*, 43(7), 1547–1554. <https://doi.org/10.1002/esp.4334>
- Hedo, J., Lucas-Borja, M.E., Wic, C., Andrés-Abellán, M. & De Las Heras, J. (2015) Soil microbiological properties and enzymatic activities of long-term post-fire recovery in dry and semiarid Aleppo pine (*Pinus halepensis* M.) forest stands. *Solid Earth*, 6(1), 243–252. <https://doi.org/10.5194/se-6-243-2015>
- Hooke, J. (2003) Coarse sediment connectivity in river channel systems: a conceptual framework and methodology. *Geomorphology*, 56(1–2), 79–94. [https://doi.org/10.1016/S0169-555X\(03\)00047-3](https://doi.org/10.1016/S0169-555X(03)00047-3)
- Kalantari, Z., Cavalli, M., Cantone, C., Crema, S. & Destouni, G. (2017) Flood probability quantification for road infrastructure: Data-driven spatial-statistical approach and case study applications. *Science of the*

- Total Environment*, 581–582, 386–398. <https://doi.org/10.1016/j.scitotenv.2016.12.147>
- Keesstra, S.D., Bagarello, V., Ferro, V., Finger, D. & Parsons, A.J. (2020) Connectivity in hydrology and sediment dynamics. *Land Degradation & Development*, 31(17), 2525–2528. <https://doi.org/10.1002/ldr.3401>
- Kumar, V. (2011) In: Singh, V.P., Singh, P. & Haritashya, U.K. (Eds.) *Elongation Ratio BT - Encyclopedia of Snow, Ice and Glaciers*. Dordrecht: Springer Netherlands, p. 257.
- López-Vicente, M. & Ben-Salem, N. (2019) Computing structural and functional flow and sediment connectivity with a new aggregated index: A case study in a large Mediterranean catchment. *Science of the Total Environment*, 651, 179–191. <https://doi.org/10.1016/j.scitotenv.2018.09.170>
- López-Vicente, M., González-Romero, J. & Lucas-Borja, M.E. (2020) Forest fire effects on sediment connectivity in headwater sub-catchments: Evaluation of indices performance. *Science of the Total Environment*, 732, 139206. <https://doi.org/10.1016/j.scitotenv.2020.139206>
- López-Vicente, M., Kramer, H. & Keesstra, S. (2021) Effectiveness of soil erosion barriers to reduce sediment connectivity at small basin scale in a fire-affected forest. *Journal of Environmental Management*, 278(Pt 1), 111510. <https://doi.org/10.1016/j.jenvman.2020.111510>
- Lucas-Borja, M.E., González-Romero, J., Plaza-Álvarez, P.A., Sagra, J., Gómez, M.E. & Moya, D. (2019) The impact of straw mulching and salvage logging on post-fire runoff and soil erosion generation under Mediterranean climate conditions. *Science of the Total Environment*, 654, 441–451. <https://doi.org/10.1016/j.scitotenv.2018.11.161>
- Marchi, L., Comiti, F., Crema, S. & Cavalli, M. (2019) Channel control works and sediment connectivity in the European Alps. *Science of the Total Environment*, 668, 389–399. <https://doi.org/10.1016/j.scitotenv.2019.02.416>
- Martínez-Murillo, J.F. & López-Vicente, M. (2018) Effect of salvage logging and check dams on simulated hydrological connectivity in a burned area. *Land Degradation & Development*, 29(3), 701–712. <https://doi.org/10.1002/ldr.2735>
- Martini, L., Faes, L., Picco, L., Iroumé, A., Lingua, E., Garbarino, M. & Cavalli, M. (2020) Assessing the effect of fire severity on sediment connectivity in central Chile. *Science of the Total Environment*, 728, 139006. <https://doi.org/10.1016/j.scitotenv.2020.139006>
- Moya, D., González-De Vega, S., García-Orenes, F., Morugán-Coronado, A., Arcenegui, V., Mataix-Solera, J. et al. (2018) Temporal characterisation of soil-plant natural recovery related to fire severity in burned *Pinus halepensis* Mill. forests. *Science of the Total Environment*, 640–641, 42–51. <https://doi.org/10.1016/j.scitotenv.2018.05.212>
- Murphy, B.P., Czuba, J.A. & Belmont, P. (2019) Post-wildfire sediment cascades: a modeling framework linking debris flow generation and network-scale sediment routing. *Earth Surface Processes and Landforms*, 44(11), 2126–2140. <https://doi.org/10.1002/esp.4635>
- Ortiz-Rodríguez, A.J., Borselli, L. & Sarocchi, D. (2017) Flow connectivity in active volcanic areas: Use of index of connectivity in the assessment of lateral flow contribution to main streams. *Catena*, 157, 90–111. <https://doi.org/10.1016/j.catena.2017.05.009>
- Ortiz-Rodríguez, A.J., Muñoz-Robles, C. & Borselli, L. (2019) Changes in connectivity and hydrological efficiency following wildland fires in Sierra Madre Oriental, Mexico. *Science of the Total Environment*, 655, 112–128. <https://doi.org/10.1016/j.scitotenv.2018.11.236>
- Panagos, P., Borrelli, P., Meusburger, K., Alewell, C., Lugato, E. & Montanarella, L. (2015) Land Use Policy Estimating the soil erosion cover-management factor at the European scale. *Land Use Policy*, 48, 38–50. <https://doi.org/10.1016/j.landusepol.2015.05.021>
- Parsons, A.J., Wainwright, J., Brazier, R.E. & Powell, D.M. (2006) Is sediment delivery a fallacy? *Earth Surface Processes and Landforms*, 31(10), 1325–1328. <https://doi.org/10.1002/esp.1395>
- Pereira, P., Francos, M., Brevik, E.C., Ubeda, X. & Bogunovic, I. (2018) Post-fire soil management. *Current Opinion in Environmental Science & Health*, 5, 26–32. <https://doi.org/10.1016/j.coesh.2018.04.002>
- Porto, P., Walling, D.E. & Callegari, G. (2009) Investigating the effects of afforestation on soil erosion and sediment mobilisation in two small catchments in southern Italy. *Catena*, 79(3), 181–188. <https://doi.org/10.1016/j.catena.2009.01.007>
- Quiñonero-Rubio, J.M., Boix-Fayos, C. & de Vente, J. (2013) Desarrollo y aplicación de un índice multifactorial de conectividad de sedimentos a escala de cuenca. *Cuadernos de Investigación Geográfica*, 39(2), 203–223. <https://doi.org/10.18172/cig.1988>
- Quiñonero-Rubio, J.M., Nadeu, E., Boix-Fayos, C. & de Vente, J. (2016) Evaluation of the effectiveness of forest restoration and check-dams to reduce catchment sediment yield. *Land Degradation & Development*, 27(4), 1018–1031. <https://doi.org/10.1002/ldr.2331>
- Ramos-Díez, I., Navarro-Hevia, J., San Martín Fernández, R., Díaz-Gutiérrez, V. & Mongil-Manso, J. (2017) Evaluating methods to quantify sediment volumes trapped behind check dams, Saldaña badlands (Spain). *International Journal of Sediment Research*, 32(1), 1–11. <https://doi.org/10.1016/j.ijsrc.2016.06.005>
- Rivas-Martínez, S., Díaz, T.E., Fernández-González, F., Izco, J., Loidi, J., Lousã, M. & Penas, A. (2002) Vascular plant communities of Spain and Portugal. Addenda to the syntaxonomical checklist of 2001. *Itinera Geobotanica*, 15(1–2), 5–922.
- Robichaud, P. R., Ashmun, L. E. & Sims, B. D. (2010) Post-Fire Treatment Effectiveness for Hillslope Stabilization. General Technical Report, RMRS-GTR-240, U.S. Department of Agriculture, Forest Service, Rocky Mountain Research Station, Fort Collins, CO.
- Robichaud, P.R., Lewis, S.A., Wagenbrenner, J.W., Brown, R.E. & Pierson, F.B. (2020) Quantifying long-term post-fire sediment delivery and erosion mitigation effectiveness. *Earth Surface Processes and Landforms*, 45(3), 771–782. <https://doi.org/10.1002/esp.4755>
- Robichaud, P.R., Wagenbrenner, J.W., Brown, R.E., Wohlgemuth, P.M. & Beyers, J.L. (2008) Evaluating the effectiveness of contour-felled log erosion barriers as a post-fire runoff and erosion mitigation treatment in the western United States. *International Journal of Wildland Fire*, 17(2), 255. <https://doi.org/10.1071/wf07032>
- Robichaud, P.R., Wagenbrenner, J.W., Lewis, S.A., Ashmun, L.E., Brown, R.E. & Wohlgemuth, P.M. (2013) Post-fire mulching for runoff and erosion mitigation. Part II: Effectiveness in reducing runoff and sediment yields from small catchments. *Catena*, 105, 93–111. <https://doi.org/10.1016/j.catena.2012.11.016>
- Romero-Díaz, A., Alonso-Sarriá, F. & Martínez-Lloris, M. (2007) Erosion rates obtained from check-dam sedimentation (SE Spain). A multi-method comparison. *Catena*, 71(1), 172–178. <https://doi.org/10.1016/j.catena.2006.05.011>
- Rulli, M.C., Offeddu, L. & Santini, M. (2013) Modeling post-fire water erosion mitigation strategies. *Hydrology and Earth System Sciences*, 17(6), 2323–2337. <https://doi.org/10.5194/hess-17-2323-2013>
- Sandercock, P.J. & Hooke, J.M. (2011) Vegetation effects on sediment connectivity and processes in an ephemeral channel in SE Spain. *Journal of Arid Environments*, 75(3), 239–254. <https://doi.org/10.1016/j.jaridenv.2010.10.005>
- Shakesby, R.A. (2011) Post-wildfire soil erosion in the Mediterranean: Review and future research directions. *Earth-Science Reviews*, 105(3–4), 71–100. <https://doi.org/10.1016/j.earscirev.2011.01.001>
- Smith, H.G., Blake, W.H. & Taylor, A. (2014) Modelling particle residence times in agricultural river basins using a sediment budget model and fallout radionuclide tracers. *Earth Surface Processes and Landforms*, 39(14), 1944–1959. <https://doi.org/10.1002/esp.3589>
- Sørensen, R. & Seibert, J. (2007) Effects of DEM resolution on the calculation of topographical indices: TWI and its components. *Journal of Hydrology*, 347(1–2), 79–89. <https://doi.org/10.1016/j.jhydrol.2007.09.001>
- Sougnéz, N., Wesemael, B. & Vanacker, V. (2011) Low erosion rates measured for steep, sparsely vegetated catchments in southeast Spain. *Catena*, 84(1–2), 1–11. <https://doi.org/10.1016/j.catena.2010.08.010>
- Stavi, I. (2019) Wildfires in Grasslands and Shrublands: A Review of Impacts on Vegetation, Soil, Hydrology, and Geomorphology. *Water*, 11(5), 1042. <https://doi.org/10.3390/w11051042>
- Tessler, N., Wittenberg, L., Malkinson, D. & Greenbaum, N. (2008) Fire effects and short-term changes in soil water repellency – Mt. Carmel,

- Israel. *CATENA*, 74(3), 185–191. <https://doi.org/10.1016/j.catena.2008.03.002>
- Thomas, I.A., Jordan, P., Shine, O., Fenton, O., Mellander, P., Dunlop, P. & Murphy, P.N.C. (2017) Defining optimal DEM resolutions and point densities for modelling hydrologically sensitive areas in agricultural catchments dominated by microtopography. *International Journal of Applied Earth Observation and Geoinformation*, 54, 38–52. <https://doi.org/10.1016/j.jag.2016.08.012>
- Turnbull, L., Hütt, M.T., Ioannides, A.A., Kininmonth, S., Poepl, R., Tockner, K. *et al.* (2018) Connectivity and complex systems: Learning from a multi-disciplinary perspective. *Applied Network Science*, 3(1), 11. <https://doi.org/10.1007/s41109-018-0067-2>
- Turnbull, L. & Wainwright, J. (2019) From structure to function: Understanding shrub encroachment in drylands using hydrological and sediment connectivity. *Ecological Indicators*, 98, 608–618. <https://doi.org/10.1016/j.ecolind.2018.11.039>
- USGS. (2004) FIREMON BR cheat sheet V4 [online]. Available http://burnseverity.cr.usgs.gov/pdfs/LAv4_BR_CheatSheet.pdf
- Vallejo, V. & Alloza, J. (2012) Post-fire management in the Mediterranean Basin. *Israel Journal of Ecology & Evolution*, 58(2), 251–264. <https://doi.org/10.1560/IJEE.58.2-3.251>
- Vieira, D.C.S., Malvar, M.C., Fernández, C., Serpa, D. & Keizer, J.J. (2016) Geomorphology annual runoff and erosion in a recently burn Mediterranean forest – the effects of plowing and time-since-fire. *Geomorphology*, 270, 172–183. <https://doi.org/10.1016/j.geomorph.2016.06.042>
- Vieira, D.C.S., Malvar, M.C., Martins, M.A.S., Serpa, D. & Keizer, J.J. (2018) Key factors controlling the post-fire hydrological and erosive response at micro-plot scale in a recently burned Mediterranean forest. *Geomorphology*, 319, 161–173. <https://doi.org/10.1016/j.geomorph.2018.07.014>
- Wagenbrenner, J.W. & Robichaud, P.R. (2014) Post-fire bedload sediment delivery across spatial scales in the interior western United States. *Earth Surface Processes and Landforms*, 39(7), 865–876. <https://doi.org/10.1002/esp.3488>
- Wohl, E., Brierley, G., Cadol, D., Coulthard, T.J., Covino, T., Fryirs, K.A. *et al.* (2019) Connectivity as an emergent property of geomorphic systems. *Earth Surface Processes and Landforms*, 44(1), 4–26. <https://doi.org/10.1002/esp.4434>
- Yochum, S.E. & Norman, J.B. (2015). Wildfire-Induced Flooding and Erosion Potential Modeling: Examples from Colorado, 2012 and 2013. 3rd Joint Federal Interagency Conference on Sedimentation and Hydrologic Modeling. Reno, Nevada, USA. <https://doi.org/10.13140/RG.2.1.4422.1923>

SUPPORTING INFORMATION

Additional supporting information may be found online in the Supporting Information section at the end of this article.

How to cite this article: González-Romero, J., López-Vicente, M., Gómez-Sánchez, E., Peña-Molina, E., Galletero, P., Plaza-Alvarez, P. *et al.* (2021) Post-fire management effects on sediment (dis)connectivity in Mediterranean forest ecosystems: Channel and catchment response. *Earth Surface Processes and Landforms*, 46(13), 2710–2727. Available from: <https://doi.org/10.1002/esp.5202>